Enhancing light-matter interaction using antenna effects

Master's thesis
by
Jenny Karlsson

LRAP-419
Lund, May, 2010

Abstract

This master's thesis explores the possibility to use a plasmonic antenna to scale a quantum computer based on rare-earth-ion-doped crystals to a large number of qubits.

To obtain a fully scalable rare-earth-ion quantum computer it is necessary to create entanglement between spatially remote qubits. This can be done using a photon pair with entangled polarization states. One single photon must act as a pi-pulse for an ion in a crystal. To enhance the interaction between the photon and the ion a toroidal microresonator in combination with an optical antenna is proposed. The microresonator can enhance the interaction time between the photon and the ion and the optical antenna can focus the evanescent field down to a sub-wavelength spot.

This report gives basic theory of quantum computing and plasmonics. The idea of how to entangle remote ions using a plasmonic antenna is presented. An optical bowtie antenna is designed and simulated using COMSOL Multiphysics®. The method is evaluated by comparison to a theoretical model for a simple case.

Simulations show that the designed antenna can enhance an evanescent field more than 1000 times at the surface of a crystal. The enhancement is enough to make a single photon act as a pi-pulse for an ion sitting at the surface. Difficulties with this approach to a scalable rare-earth-ion quantum computer are discussed and further investigations are suggested.

Sammanfattning

Detta examensarbete utforskar möjligheten att använda en plasmonisk antenn för att skala upp en kvantdator baserad på kristaller dopade med joner av sällsynta jordartsmetaller till ett stort antal kvantbitar.

För att skapa en fullt skalbar kvantdator baserad på jordartsjoner är det nödvändigt att sammanfläta kvanttillstånden hos rumsligt separerade kvantbitar. Detta är möjligt genom att använda ett fotonpar med sammanflätade polarisationstillstånd. En enda foton måste motsvara en pi-puls for en jon som sitter i en kristall. Enligt förslaget som presenteras i rapporten kan en toroid-formad mikroresonator i kombination med en optisk antenn användas för att förstärka interaktionen mellan en foton och en jon. Mikroresonatorn kan förlänga interaktionstiden mellan fotonen och jonen och den optiska antennen kan fokusera det evanescenta fältet till en punkt mindre än ljusets våglängd.

I rapporten ges grundläggande teori för kvantdatorer och plasmonik. Idén för att sammanfläta separerade joner presenteras. En optisk antenn utformas och simuleras i COMSOL Multiphysics®. Metoden utvärderas genom en jämförelse med en teoretisk beräkning för ett enkelt fall.

Simuleringarna visar att den utformade antennen kan förstärka ett evanescent fält mer än 1000 gånger på ytan av en kristall. Förstärkningen är tillräcklig för att skapa en pi-puls från en enda foton för en jon som sitter på ytan av kristallen. Svårigheter med det beskrivna angreppssättet för att skala en kvantdator baserad på jordartsjoner diskuteras och ytterligare undersökningar föreslås.

Contents

Chapter 1

Introduction

The first electronic computers were developed in the 1930s. From the beginning they were huge machines with less capabilities than the pocket calculators of today. Since the invention of the transistor in the 1940s the development of smaller and faster computers has been amazingly rapid. Today it's hard to imagine a world without computers, they shape our society and lives in a way no one could have expected.

The rapid development of the computer is only one example of how modern technology is getting smaller and faster. Eventually single molecules or particles will act as electronic components. It will be necessary to be able to manipulate and control quantum systems if we want to make our circuits and electronic components smaller.

At the same time as computers get smaller we also have an increasing demand on efficiency and speed. The fastest possible way to communicate is by using light. Today optical fibers are used to send information over large distances. Photonics is a growing field of science, not the least shown by the Nobel prizes in physics of 2009.

A quantum computer could offer new ways to solve problems, sometimes with an exponential speed up compared to classical computers. To take advantage of the sometimes weird properties of quantum systems is a natural step in the development of the computer systems of tomorrow.

As electronics is replaced by optics the demand for small components to control and manipulate light is growing. Plasmonics is a very exciting field in the overlap between electronics and photonics. Plasmonics might make it possible to design optical circuits, antennas or even transistors comparable with the electronic versions of today.

Within the scope of this thesis I have the privilege to work with all the above mentioned fields of physics. Quantum mechanics, photonics and plasmonics are all fields with great potentials to shape the future of technology.

The aim for this diploma project is to improve the scalability of a rare-earth-ion quantum computer system by making it possible to entangle remote ions. This is done by the design of an optical antenna to enhance the field from a single photon.

1.1 Outline

This thesis is structured as follows.

Chapter 2,3 and 4 give the background and purpose of my work. Chapter 2 and 3 contain the theory of quantum computing necessary to understand the aim of my work. Chapter 4 focuses on how to make a quantum computer scalable to a large number of qubits and motivates the use of

an optical antenna.

Chapter 5, 6 and 7 introduce the theory of surface plasmons and optical antennas. The aim is to give a theoretical framework and background to my simulations.

Chapter 8 describes the method used for designing and evaluating an optical antenna. The numerical method, geometry and modeling parameters are given.

Chapter 9 gives a comparison between theory and simulations for a simple case. This is used to identify weaknesses and error sources of the method and to evaluate if the chosen method is suitable for this kind of simulations.

Chapter 10 and 11 present the design and properties of an optical bowtie antenna based on simulations.

Chapter 12 deals briefly with some practical considerations as well as remaining questions not investigated within the scope of this thesis.

Finally, chapter 13 gives the conclusion and a brief outlook based on this work.

Chapter 2

Quantum computing

What is a quantum computer? How does it work and why do we need it?

In this chapter I will give a brief introduction to the field of quantum computing. I intend to answer the questions above in a way that should be accessible to someone who has never heard of quantum computers before.

A quantum computer works in a way very similar to a regular computer. The big difference lies in the smallest pieces of information that is stored and processed in the computer. The quantum-bit, or qubit, makes use of quantum mechanics to store superpositions of 1s and 0s rather than just a 1 or a 0 as in a regular bit. This rather simple difference makes it possible to run entirely different algorithms on the quantum computer.

2.1 A very brief review of computer language

Most people know that a regular computer, like the one I'm using right now, works by manipulating 1s and 0s. All information is stored and processed as binary digits. One such piece of information that can be either a 1 or a 0 is called a *bit*. If you put eight bits together you will get a so called *byte* of information. For example my hard drive can store 300 gigabytes, which is $2.4 \cdot 10^{12}$ bits.

The processor in a computer performs operations on bits. These operations are executed in so called *gates*. For example a NOT-gate will switch a 0 to a 1, and a 1 to a 0. This can be written:

$$\text{NOT } 1 \rightarrow 0$$

$$\text{NOT } 0 \rightarrow 1$$

More complicated gates can have two inputs, so called two-bit gates. One example of a two-bit gate is the controlled NOT gate, or C-NOT gate for short. It performs a NOT operation on bit two on the condition that bit one is a 1. If bit one is a 0, nothing happens. Bit one is called the control bit while bit two is the target bit

$$\text{C-NOT } 1_1 0_2 \rightarrow 1_1 1_2$$

$$\text{C-NOT } 0_1 0_2 \rightarrow 0_1 0_2$$

2.2 Quantum bits

A quantum computer works in a way very similar to a regular computer by manipulating 1s and 0s. But this time we use a special feature of quantum mechanical systems: they can not only be in

state 1 or in state 0 as a regular bit, but also in a linear combination of 1 and 0. This special kind of bit is called a quantum-bit, or *qubit*. A linear combination, or *superposition*, between different states means that the qubit can be for example 30% in state 0 and 70% in state 1. This can be written with Dirac notation in the following way:

$$|\psi_{qubit}\rangle = \alpha\,|0\rangle + \beta\,|1\rangle$$

$$|\alpha|^2 + |\beta|^2 = 1$$

α and β are the complex amplitudes of the superposition.

When we measure which state a qubit is in, the wave function of the qubit, $|\Psi_{qubit}\rangle$, will collapse to one of the states $|0\rangle$ or $|1\rangle$. We will not be able to measure the superposition state. However, $|\alpha|^2$ is the probability to find the qubit in state $|0\rangle$ and $|\beta|^2$ is the probability to find the qubit in state $|1\rangle$, so if we can create the same superposition many times, or in many qubits, repeated measurements can give us an idea of what state the qubit was in before the measurement.

When two qubits are in superpositions of $|0\rangle$ and $|1\rangle$, the state of the two-qubit-system can be written:

$$|\psi_1\rangle \otimes |\psi_2\rangle = (\alpha_1\,|0\rangle + \beta_1\,|1\rangle)_1 \otimes (\alpha_2\,|0\rangle + \beta_2\,|1\rangle)_2 \tag{2.1}$$

$$= \alpha_1\alpha_2\,|0\rangle_1\,|0\rangle_2 + \alpha_1\beta_2\,|0\rangle_1\,|1\rangle_2 + \beta_1\alpha_2\,|1\rangle_1\,|0\rangle_2 + \beta_1\beta_2\,|1\rangle_1\,|1\rangle_2 \tag{2.2}$$

The basis states are the four different combinations $|0\rangle_1\,|0\rangle_2$, $|0\rangle_1\,|1\rangle_2$, $|1\rangle_1\,|0\rangle_2$ and $|1\rangle_1\,|1\rangle_2$. To make the notation a bit less messy the states can be written within a single ket as $|00\rangle$, $|01\rangle$, $|10\rangle$ and $|11\rangle$. Here it is assumed that the first number within each ket referrers to qubit one and the second number to qubit two. I will however not use this convention in the following chapter, to emphasize that we have two separate qubits.

2.3 Quantum gates

A quantum computer is a collection of qubits, just like a normal computer is a collection of bits. A quantum computer performs operations on qubits just like a regular processor manipulate bits. Quantum gates are used to change the states of qubits in a desirable way. Mathematically gates are operators that operate on the wave function of the qubits involved. For example a NOT-gate in a quantum computer acts in the following way:

$$\text{NOT}\ \ |0\rangle \rightarrow |1\rangle$$

$$\text{NOT}\ \ |1\rangle \rightarrow |0\rangle$$

A NOT-gate will take a qubit that was initially 30% in state 0 and 70% in state 1 to 70% in state 0 and 30% in state 1. More generally:

$$\text{NOT}\ \ (\alpha\,|0\rangle + \beta\,|1\rangle) \rightarrow \alpha\,|1\rangle + \beta\,|0\rangle$$

Two-qubit gates are slightly more complicated than their classical counterparts, because both input qubits can be in superpositions of the two states $|1\rangle$ and $|0\rangle$. A C-NOT-gate can be viewed as an operator that acts on the basis states in a way very similar to the classical gate:

$$\text{C-NOT}\ \ |1\rangle_1\,|0\rangle_2 \rightarrow |1\rangle_1\,|1\rangle_2$$

$$\text{C-NOT}\ \ |0\rangle_1\,|0\rangle_2 \rightarrow |0\rangle_1\,|0\rangle_2$$

If two qubits are in superpositions of the states $|1\rangle$ and $|0\rangle$ a two-qubit-gate *entangles* the qubits. This means that we can no longer separate the qubits as two quantum systems, but has to take both into account. For example a C-NOT-gate will entangle qubit one and two in the following way:

$$\text{C-NOT}\ \ (|\psi_1\rangle \otimes |\psi_2\rangle) = \text{C-NOT}\ \ (\alpha_1\,|0\rangle + \beta_1\,|1\rangle)_1 \otimes (\alpha_2\,|0\rangle + \beta_2\,|1\rangle)_2$$

$$= \text{C-NOT } (\alpha_1\alpha_2 |0\rangle_1 |0\rangle_2 + \alpha_1\beta_2 |0\rangle_1 |1\rangle_2 + \beta_1\alpha_2 |1\rangle_1 |0\rangle_2 + \beta_1\beta_2 |1\rangle_1 |1\rangle_2)$$
$$\rightarrow \alpha_1\alpha_2 |0\rangle_1 |0\rangle_2 + \alpha_1\beta_2 |0\rangle_1 |1\rangle_2 + \beta_1\alpha_2 |1\rangle_1 |1\rangle_2 + \beta_1\beta_2 |1\rangle_1 |0\rangle_2$$

The result of the operation makes the superposition in qubit one depend on the superposition in qubit two in such a way that the expression above can no longer be factorized into a product of one wave function for qubit one and another for qubit two. The qubits are entangled.

2.4 Quantum algorithms

A quantum computer is a collection of qubits that we can perform operations on. A qubit is a quantum mechanical system that can be in any superposition of the states $|0\rangle$ and $|1\rangle$. The states can be for example energy levels in an atom, spin states of an electron or polarization states of a photon.

After many gate operations a large number of qubits in a quantum computer will be entangled. The quantum computer can be viewed as one single quantum system rather than many small qubits. This huge quantum system is in a superposition between 2^N different states, where N is the number of entangled qubits.

A regular computer can also be in 2^N different states, where N is the number of bits stored in the processor. So what have we gained by making things more complicated? Each moment a regular computer is in one single state, while the quantum computer is in a superposition of all possible states. This makes it possible to run what would on a regular computer be many different calculations in parallel.

An algorithm is a set of operations used to solve a specific problem. A quantum computer could run any algorithm designed for a regular computer. There is also a special class of algorithms, *quantum algorithms*, designed for quantum computers. A quantum algorithm makes use of the special properties of the qubits, to solve a problem using less operations than would be possible on a regular computer.

The most well-known quantum algorithm is Shor's algorithm for factorizing large integers, discovered in 1994 by Peter Shor [1]. It runs at least exponentially faster than any known classical algorithm that do the same thing. Shor's algorithm is interesting because it could be used to break the cryptography scheme RSA, widely used for protecting web pages, email etc. RSA uses the fact that factorizing very large integers is impossible in practice, it simply takes too much time. With a quantum computer using Shor's algorithm it would be a lot faster and the RSA scheme would not be safe. A new type of cryptography would be needed, for example *quantum cryptography* [2].

Shor's algorithm takes advantage of the fact that a collection of qubits can be in a superposition of many different states. This can be used to do many things in parallel, for example evaluate a function $f(x)$ for many different values of x at the same time.

There are several other quantum algorithms that could offer more than polynomial speed up compared to the algorithms used today, for example simulations of quantum systems in physics or chemistry.

2.5 Quantum computer hardware

So far, a qubit is a theoretical entity that we can operate on by using equally theoretical gates. To make a real quantum computer however, we need to construct hardware to support our qubits and gates. This can be done in many different ways, but is not an easy task. In 2000 David DiVincenzo at IBM listed five requirements for implementing a quantum computer, [3]:

A scalable system of qubits A qubit can be any quantum mechanical two-level system that

can be manipulated and controlled with required precision. The system needs to be scalable to a large number of qubits to be able to make use of the different algorithms available.

Ability to initialize qubits to a known value Before starting a sequence of operations we need to know what state the qubits are in.

A long coherence time (compared to the gate operation time) The quantum mechanical system used as a qubit must be coherent during the time it is used. A much simplified description of what it means for a qubit to be coherent is that the superposition between the two possible states is well-defined. Without coherence, the quantum computer will be reduced to a regular computer.

A set of gates To run algorithms on a quantum computer we need to be able to control the qubits and perform operations on them. It can be shown that all possible gates can be built from the C-NOT gate together with a set of one-qubit gates.

Qubit specific read-out To get a result from our computations we need to be able to measure the states of our qubits one by one.

Work has been done to implement quantum computer schemes in many different physical systems. Qubits can for example be represented by nuclear spin states using NMR, polarization states in photons controlled with linear optics, electron spins in quantum dots or energy levels of trapped ions. So far no experimental system has all the desired properties to function as a large scale quantum computer.

Few qubit operations have been demonstrated in a number of systems including the NMR-technique [4] [5], Ion traps [6] [7] and optical systems [8]. Shor's algorithm was demonstrated for the first time in 2001 by factorizing 15 using the NMR-technique [9] and again in 2007 using photon polarization states [10]. Small scale qubit interaction have recently been shown in solid state systems using superconducting circuits which are promising for future larger scale quantum-circuits [11].

In this thesis I will only consider quantum computing using rare-earth-ion-doped crystals which will be described in more detail in the following chapter. Investigations concerning enhanced light-matter interaction can however be useful in a number of different implementations and also within other research fields than quantum computing.

Chapter 3

Quantum computing using rare-earth-ion-doped crystals

As was seen in the previous chapter there are several potential systems for implementing a quantum computer. In this chapter I will describe how quantum computing can be done using rare-earth-ion-doped crystals. The scheme was first proposed by Ohlsson et al. in 2001, [12].

The hardware for a rare-earth-ion quantum computer is a crystal doped with rare-earth-ions, for example Pr^{3+}:Y_2SiO_5. Two hyperfine levels in the ions are used as the states $|0\rangle$ and $|1\rangle$, as in figure 3.1. The qubits can be manipulated using an intermediate optical transition to a higher energy state $|e\rangle$.

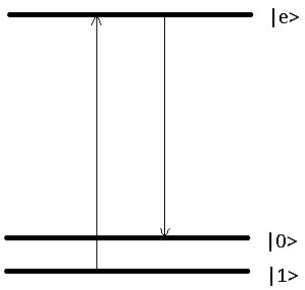

Figure 3.1: Two hyperfine levels in a rare-earth ion can be used as the two states of a qubit. The figure is not to scale.

3.1 Principles of rare-earth-ion quantum computing

One of the big advantages of using rare-earth-ions doped into a host crystal is the long coherence times of the ions. The partly filled electron shells used to perform qubit operations are shielded from the environment by outer lying filled shells. The electronic state coherence time in Pr^{3+}-ions is about 100 μs and the hyperfine states used as qubits have coherence times of about 500 μs. There are techniques to extend the coherence times further, for example by using magnetic fields. The long lifetime of the ions makes the homogeneous absorption profile narrow, about 3 kHz for Pr^{3+}-ions, [13].

When rare-earth-ions are doped into a host crystal they randomly replace host ions in the crystal lattice. Doing so they alter the local electric field of the crystal lattice where they sit. The random change of the electric field causes the ions to shift their energy levels in a random manner, forming

a wide inhomogeneous absorption profile. For the Pr^{3+}:Y_2SiO_5 the inhomogeneous line width is about 5 GHz, [13].

The narrow homogeneous line width in combination with the wide inhomogeneous line width makes it possible to address different subgroups of ions by tuning the laser to a specific frequency within the inhomogeneous profile. Each such ensemble of ions can act as a qubit, as marked with colours in the figure 3.2.

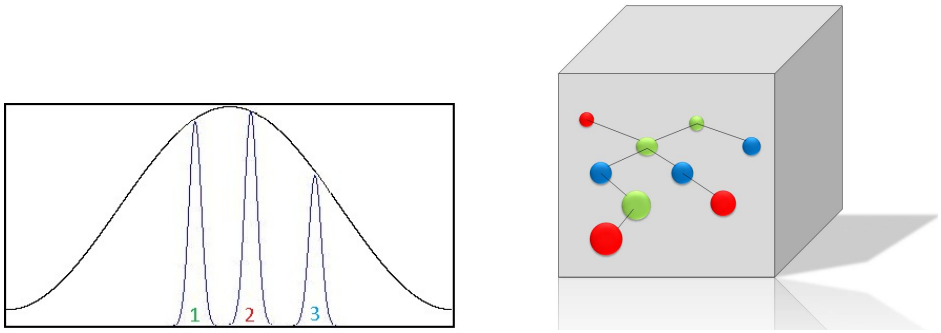

(a) (b)

Figure 3.2: Subgroups of ions within the inhomogeneous absorption profile can be used as ensemble qubits.

To create two-qubit gates the qubits need to interact with each other. Two ions sitting close to one another can interact via their permanent dipole moments. When one qubit is in the excited state the change in permanent dipole moment will shift the resonance frequencies of the surrounding qubits. This can be used to create entanglement between close sitting qubits.

A more detailed description of rare-earth-ion-doped crystals used for quantum computing can be found in [14].

3.2 Initialization of ensemble qubits

To be able to coherently control each qubit with the laser we want to define narrow frequency regions to represent each qubit. When setting the laser to a specific frequency we want to interact with ions in one qubit but not with other ions lying close to that qubit in frequency. In this sense we want to isolate a narrow frequency range within the inhomogeneous profile for each qubit.

By first burning a spectral pit in the absorption profile we can remove all ions that we don't want to interact with from a certain frequency interval. This can be done by simply scanning the laser back and forth over a limited frequency range. To make the pit as wide as possible and to move close lying ions as far away from the pit as possible an optimized sequence of laser pulses is used. The maximum width of the pit is limited by the splitting between the hyperfine levels in the ground state and in the excited state. A sequence of burnback pulses are then used to transfer ions back into the pit in well-defined narrow peaks. Each peak represents one qubit as shown in figure 3.3 and can be addressed independently with the laser as long as the separation between the peaks is large enough, [15].

After the burnback sequence each peak still has a certain inhomogeneous width. This small difference in resonance frequency between the different ions in a qubit makes it difficult to coherently transfer all ions to the same quantum state. A chirped pulse, for example a so called sechyp pulse, can be used to overcome this problem, [16].

All ions within one ensemble qubit must interact with the other qubits to be useful. For two ions to interact they need to sit sufficiently close to each other in the crystal. Ions that are not interacting with the other qubits can be found and transferred to a third hyperfine level called the auxiliary

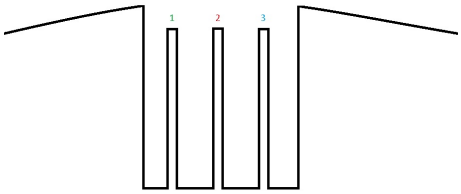

Figure 3.3: By burning a spectral pit and moving ions back into the pit in a controlled way we can create narrow separated peaks acting as qubits.

state. When placed in this state the ion will not be addressed by the laser and will not take part in quantum computations, [17].

3.3 Scalability of the ensemble qubit quantum computer

For an ensemble qubit it is necessary for all ions within the ensemble to interact with at least one ion from each of the other qubits. The ions that do not interact with the other qubits are put in the auxiliary state and are not used.

If the probability for an ion to interact with an ion from another qubit is p, then the probability to interact with at least one ion from each of the other qubits scales as p^{n-1} where n is the number of qubits in the quantum computer. This probability is very small for a large number of qubits. With $p \approx 1\%$ in a five-qubit computer only 1 out of 10^8 ions in each qubit are useful, [13].

There are ways to improve the scalability by for example working with a very high dopant concentration or by using a so called bus-ion to mediate between qubits, [18]. Even then the ensemble qubit approach is not practical for a large number of qubits. To be able to make a larger quantum computer single-ion qubits might be the best choice.

3.4 Single-ion qubits

One way to improve the scalability of the rare-earth quantum computer is to use single ions as qubits. One single ion could interact with several other ions sitting close to each other in the crystal. The surrounding ions can in turn interact with other ions and we can use branched chains of clustered ions that can interact and mediate information.

The problem with this approach is to read out the state of single qubits. It must also be possible to identify and address the ions used as qubits independently. There are proposed ways to do this.

To be able to read out the state of a single ion qubit a special readout ion can be used. The readout ion can be an ion with a short excited state lifetime where it is possible to cycle a transition many times and get a stronger signal. The qubit ions interact with the readout ion through their permanent dipole moments. The readout ion can be shifted in or out of resonance depending on the state of a nearby qubit.

Ce^{3+} seems to be a good choice for a readout ion. The excitation wavelength of 371 nm is well separated from the qubit transitions so that the state of the qubits will not be affected by the readout signal. The Ce-transition has a narrow line width which makes it possible for a Ce-ion to be shifted out of resonance when interacting with a qubit, [18].

A find and search scheme can be applied to find the resonance frequencies of ions that sit close to a readout ion and then further extend the number of qubits in branched chains from the readout ion.

When scaling the quantum computer to more and more qubits, there will eventually be an ion with the same resonance frequency as an already existing qubit ion. This limits the number of qubits in the quantum computer. There are ways to shift the resonance frequencies and extend the scalability further by for example putting small and closely spaced electrodes on the surface of the crystal, [18].

Eventually, when scaling the quantum computer to a very large number of qubits, it's necessary to entangle spatially remote qubits, [13]. An effective way to entangle two ions at different locations would be a big step forward to a scalable rare-earth-ion quantum computer. This will be discussed more in the next chapter.

3.5 Experimental realization of a rare-earth quantum computer

Experiments have been done to investigate the possibilities to use rare-earth-ion-doped crystals as hardware for quantum computing. Especially Pr^{3+}:Y_2SiO_5 and Eu^{3+}:Y_2SiO_5 have been studied. The crystal is cooled to temperatures below 4 K to avoid thermal disturbance and achieve a long coherence time for the ions. This can be done by placing the crystal in liquid helium inside a cryostat. The laser needs to have a very narrow line width in order to manipulate individual qubits and also need to be very stable.

Ensemble qubits have been prepared and characterized using quantum state tomography, [19], [20]. Single qubit operations have been demonstrated with a fidelity of about 90% and the dipole-dipole interaction between qubits have been measured, [19], [17].

Chapter 4

Scalability to a large number of qubits

As was explained in the previous chapter one of the problems with a rare-earth-ion quantum computer is the difficulty to scale the computer to a large number of qubits. A single-ion qubit approach offers a better scalability but to achieve a large scale quantum computer we need to entangle remote clusters of qubits. There has been a couple of different ideas of how to do this during the process of my work and what I will present in this chapter is the most resent idea.

The idea of using small registers of a few qubits and remotely entangle many such registers is not only interesting for rare-earth quantum computing, but also for other implementations, [21].

4.1 A quick review of light-matter interaction

Coherent interaction between light and matter can be described using the Bloch equations and conveniently visualized in the Bloch sphere. The Bloch equations is a system of differential equations describing the evolution of three coordinates u, v and w.

$$\dot{u} = \delta v - \frac{\Gamma}{2}u$$

$$\dot{v} = -\delta u + \Omega w - \frac{\Gamma}{2}v$$

$$\dot{w} = -\Omega v - \Gamma(w-1)$$

A superposition between two quantum mechanical states can be described with one amplitude relationship determining the probability to find the system in one level or the other and one phase relationship between the two superpositioned wave functions of the levels. In the Bloch equations w describes the amplitude relationship with $w = -1$ meaning that the system is in the ground state and $w = 1$ meaning the system is in the excited state. The coordinates u and v determines the phase relationship between the states.

The detuning, δ, is the difference between the frequency of the applied field and the energy splitting between the two states $|1\rangle$ and $|2\rangle$. Γ is the damping rate of the system.

Ω is the so called Rabi frequency of the system. The Rabi frequency describes the coupling between two levels, $|1\rangle$ and $|2\rangle$, in the presence of an electromagnetic field with amplitude $\mathbf{E}_0$.

$$\Omega = \frac{\langle 1| e\mathbf{r} \cdot \mathbf{E}_0 |2\rangle}{\hbar}$$

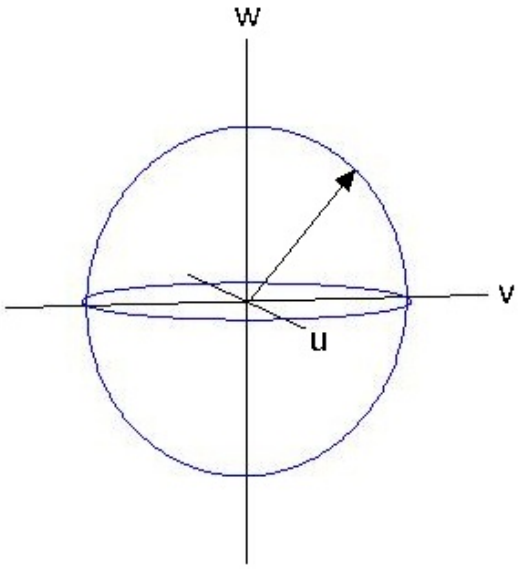

Figure 4.1: The state of a quantum system can be visualized on the Bloch sphere.

If the amplitude $\mathbf{E}_0$ changes slowly and is approximately constant over the volume of the system we can move it out of the braket and write:

$$\Omega = \frac{\mathbf{E}_0}{\hbar} e \langle 1| \mathbf{r} |2\rangle = \frac{\mathbf{E}_0 \mu}{\hbar}$$

where $\mu = e \langle 1| \mathbf{r} |2\rangle$ is the dipole moment of the transition.

The vector (u, v, w) is called the Bloch vector. For a system without losses the magnitude of the Bloch vector is always equal to one and as the system evolves with time the Bloch vector will move on a unit sphere as in figure 4.1. This unit sphere is called the Bloch sphere.

In a system with no detuning or losses the wave function of the system will oscillate between the ground state and the excited state with the Rabi (angular) frequency. This phenomenon is called *Rabi flopping*. The pulse area of a light pulse, Ωt, is in the case with no detuning the angle traversed by the Bloch vector in the Bloch sphere during the pulse. For a so called pi-pulse $\Omega t = \pi$ the system has then moved 180 degrees in the Bloch sphere, for example from the ground state to the excited state as in figure 4.2.

A more detailed description of the Bloch formalism can be found in [22].

4.2 Remote ion entanglement

The rare-earth-ions doped into a crystal are sitting in two different sites in the crystal structure. The dipole moments of the ions are lined up in two different directions. By orienting the crystal in the right way with light incident in the plane spanned by the dipole moments of the ions, it is possible to get a high absorption for horizontally polarized light, say, and no absorption for vertically polarized light.

By sending a photon pair with opposite entangled polarization states to two different crystals oriented in the same way we know that one photon can be absorbed and one will pass through the

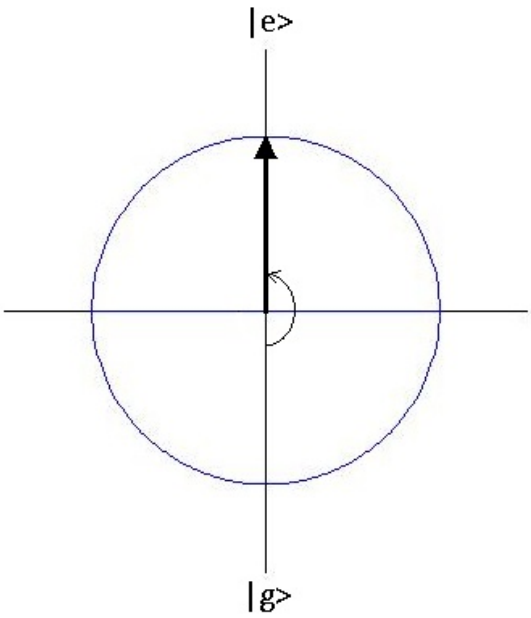

Figure 4.2: A pi-pulse moves a quantum system an angle pi from the ground state to the excited state.

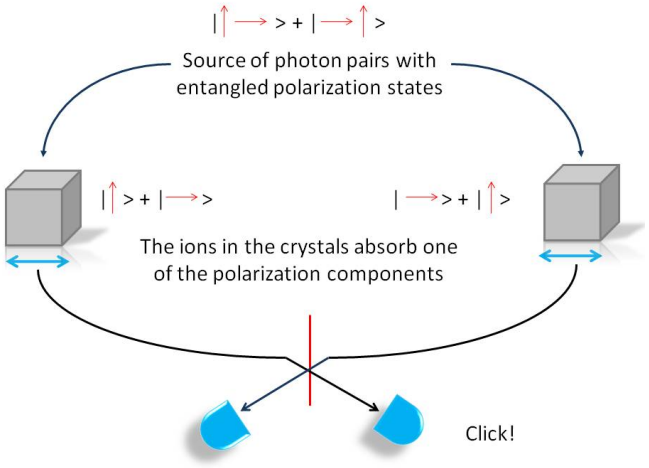

Figure 4.3: Ions sitting in different crystals get entangled by absorbing one of the polarization components of an entangled photon pair.

crystal unaffected. When crossing the two photon paths in a 50/50 beam splitter any information on which path the photon took and hence which crystal absorbed a photon is lost. This allows two ions in the different crystals to be entangled. The principal set-up can be seen in figure 4.3.

If we detect two photons after the beam splitter we know that none of the photons were absorbed and we can re-do the procedure. Even if we only detect one photon there can still be losses and errors in the process. Using efficient error correction schemes we can allow the error probability to be as high as a few percent if the error probability within each cluster is small, [21].

To coherently excite an ion we need to apply a pi-pulse. The photon should be absorbed by an

ion in the crystal with a probability close to 100%. To achieve a single photon pi-pulse we need to enhance the interaction between the photon and the ion.

The so called *communicator ion* used to create entanglement between two crystals do not need to be the same kind of ion that is used for performing quantum computation. One way of achieving a strong interaction is by choosing an ion with a large transition dipole moment. The lifetime of the communicator ion is not as important as for the qubit ions, but we need the coherence time to be long enough to create entanglement and interact with a qubit ion before information is lost.

4.3 Enhancing light-matter interaction

To be able to entangle remote ions using the idea presented above one single photon should act as a pi-pulse for an ion. For this to be possible we must increase the pulse area of the photon-ion interaction. This can be done by increasing the interaction time t and by increasing the Rabi frequency Ω.

4.3.1 Using a toroidal microresonator to increase the interaction time

The interaction time can be increased by using a resonator of some kind. A toroidal microresonator can have a very high Q-value and a small mode volume which allows for strong coupling to atoms or ions. It is also relatively easy to fabricate and has very promising properties for further improvements.

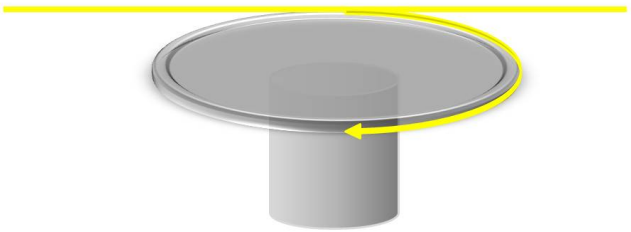

Figure 4.4: A toroidal microresonator can have a very high Q-value and a small mode volume.

A photon can be coupled into a small resonator with a very high efficiency (>99.9%) using a tapered waveguide, [23]. Q-values of 10^8 have been demonstrated for 852 nm, and values as high as 10^{10} might be possible, [24]. The lifetime of the cavity at 600 nm with a Q-value of 10^8 is:

$$\tau = \frac{Q}{\omega_0} = \frac{\lambda Q}{2\pi c} \approx 30\text{ns}$$

For a Q-value of 10^{10} the lifetime would be about 3 μs.

If the crystal is placed close to the surface of the microtoroid the ions will interact with the evanescent field from the resonator. In ref [25] experiments with cesium atoms interacting with toroidal microresonators gave a Rabi frequency of 100 MHz 45 nm away from the toroidal surface.

In ref [24] the best possible scenario when a cesium atom is placed at the point of highest field strength outside the microresonator is considered. A Rabi frequency of 1 GHz is stated as possible with currently available microresonators and even higher Rabi frequencies can be obtained by optimizing the shape and size of the resonator. The coupling strength between the atom and the resonator is higher for a smaller resonator with a smaller mode volume, but a smaller resonator can at the same time give a lower Q-value. For a toroidal microresonator with a Q-value of 10^8 a Rabi frequency as high as 5.7 GHz is stated as achievable by optimizing the shape of the toroid.

All the above mentioned Rabi frequencies are for the D_2-transition ($6^2S_{1/2}$ - $6\ ^2P_{3/2}$) in cesium atoms at 852 nm. This transition has a dipole moment of $\mu_{cs} = 3.8 \cdot 10^{-29}$ C m, [26]. The dipole moment of the strongest $^3H_4$ - $^1D_2$ transition in Pr^{3+}:Y_2SiO_5 is three orders of magnitude lower; $\mu_{pr} = 3.7 \cdot 10^{-32}$ C m, [15]. This also implies that the Rabi frequency will be three orders of magnitude lower.

Achievable Rabi frequencies

Cesium	Pr^{3+}
100 MHz	100 kHz
1 GHz	1 MHz
5.7 GHz	5.7 MHz

100 kHz should be possible to achieve by placing the crystal very close to the microresonator surface. The value is calculated for an ion sitting 45 nm away from the surface. We then need to place the crystal less than 45 nm from the resonator, how close depends on how deep into the crystal the communicator ion is sitting.

1 MHz might be possible if we can put the crystal even closer to the toroid, probably within a few nm from the surface. We would need to use an ion sitting very close to the crystal surface.

5.7 MHz is dependent on the fabrication of a smaller optimized microresonator with the properties predicted in [24]. It also depends on the possibility of putting the crystal extremely close to the surface of the resonator and using a communicator ion close to the crystal surface.

Using the lifetimes and Rabi frequencies mentioned above we can get an idea of the achievable single-photon pulse areas.

Pulse area $\Omega\tau$:

$\Omega \downarrow \tau \rightarrow$	30 ns	3 μs
100 kHz	0.003	0.3
1 MHz	0.03	3
5.7 MHz	0.171	17.1

The case of a 5.7 MHz Rabi frequency and a lifetime of 3μs is not realistic since the such an optimized resonator with a very small mode volume would not have a Q-value of 10^{10}.

The case of a 1 MHz Rabi frequency together with a long resonator lifetime is not entirely out of question but is dependent on the fact that we need to use ions very close to the surface of the crystal. In this case we are very close to achieving a pi-pulse.

For all other cases we need to enhance the evanescent field from the resonator where the ion is sitting to achieve a pi-pulse. The realistic case of 100 kHz Rabi frequency and a lifetime of 30 ns would require that we could focus the field enough to obtain a field enhancement of 10^3 where the ion is sitting. With a higher Q-value an enhancement of 10 times might be enough.

4.3.2 Increasing the Rabi frequency by focusing light to a sub-wavelength spot

Antennas have been used to transmit and receive electromagnetic waves since the end of the 19th century. Many different types of antennas has been designed for more or less specialized purposes.

Receiving antennas in the radio frequency regime can easily focus radiation down to spots much smaller than the wavelength.

With an increasing ability to manufacture very small metal structures antennas operating at optical wavelengths have received much attention. Small antenna structures can focus light down to spots much smaller than the wavelength with very high field strengths as a result.

This work aims to design an optical antenna suitable for scaling a rare earth quantum computer, and investigate if such an antenna can be used to enhance the electric field at a crystal surface enough to achieve a single photon pi-pulse. The requirements for such an antenna are listed below.

High field enhancement An enhancement of the evanescent field from the resonator between 10 and 1000 times is needed to achieve a single photon pi-pulse.

Low loss We can tolerate losses and errors of a few percent in the entanglement process. This is not very much so an antenna with as low loss as possible is desirable.

Polarization dependence We only want to absorb one of the linear polarization components of light. The antenna should not absorb, scatter or modify the other polarization component.

Field penetration into the crystal Ions sitting inside the crystal are well shielded from the environment with long coherence times as a result. Ions close to the surface might not have the coherence time needed to perform gate operations. The field should be enhanced where the communicator ions is sitting, below the crystal surface.

Coherence of the ions The antenna should not destroy the coherence properties of ions close by. This might be a tricky demand to satisfy, since an increased absorption often also implies increased emission.

In the following chapters I will present the theory needed to understand and design an optical antenna.

Chapter 5

Optical properties of metals

Metals are widely used for guiding and manipulating electromagnetic waves. A metal wire can transport power in the form of currents and voltages and a metal antenna can transmit or receive radio waves. But we don't use metals as much when it comes to optical frequencies. You never see a pair of glasses with metal lenses to focus light or a metal wire to transport the sunlight to your favorite spot in the sofa.

Metals are often used as jewelry or decoration because of the shiny beautiful surfaces. The high reflectivity implies that light does not travel through metals. Can metals still be used to transport and focus light?

In this chapter I will investigate how a metal behaves at optical wavelengths. I will deduce the simple Drude model and show that light can indeed travel through and along the surface of the metal under certain circumstances.

5.1 Sign convention

When describing propagating electromagnetic waves there are two different sign conventions in use. A time harmonic electric field $\mathbf{E}$ can be written as the real part of a complex field:

$$\mathbf{E}(\mathbf{r},t) = \mathbf{E}(\mathbf{r})cos(\omega t) = \mathrm{Re}(\mathbf{E}_c(\mathbf{r})e^{i(\omega t - k_x x)})$$

or equivalently

$$\mathbf{E}(\mathbf{r},t) = \mathbf{E}(\mathbf{r})cos(\omega t) = \mathrm{Re}(\mathbf{E}_c(\mathbf{r})e^{-i(\omega t - k_x x)})$$

The difference in sign convention may seem unimportant but will be carried on to many different formulas and variables. For example the dielectric constant of a lossy material will have a positive or negative imaginary part depending on the sign convention used. This is important to keep in mind when looking up material properties in literature.

I have chosen to follow the sign convention used by Maier [27], as well as many textbooks in optics. I write the complex electric field:

$$\mathbf{E} = \mathbf{E}_0 e^{i(k\mathbf{r} - \omega t)}$$

This implies that a lossy material will have a positive imaginary part of the permittivity.

Unfortunately the simulation software used in this thesis, Comsol Multiphysics®, uses the opposite convention which might cause some confusion.

5.2 The Drude Model

A simple way of modeling the interaction between an electric field $\mathbf{E}$ and the charges inside a material is by considering the equation of motion of the electrons. The local electric field causes a force on the electrons. Ignoring the difference between the local field and the applied field, the force can be written $\mathbf{F} = -e\mathbf{E}$. We assume that the electrons are bound by a nucleus that acts like a restoring force proportional to the displacement $\mathbf{x}$ with spring constant κ. We also assume a frictional force proportional to the velocity $\dot{\mathbf{x}}$ of the electrons and the collusion frequency γ.

$$m\ddot{\mathbf{x}} = -e\mathbf{E} - \kappa\mathbf{x} - m\gamma\dot{\mathbf{x}}$$

By assuming a harmonic time dependence of the complex field $\mathbf{E}(t) = \mathbf{E_0}e^{-i\omega t}$, where $\mathbf{E}_0$ is the complex amplitude of the field, we can easily get a solution for $\mathbf{x}$ [30]:

$$\mathbf{x}(t) = \frac{\frac{e}{m}}{\omega^2 + i\omega\gamma - \omega_0^2}\mathbf{E}(t)$$

We define $\omega_0 = \sqrt{\frac{\kappa}{m}}$ as the resonance frequency of the electron-nucleus spring. For a metal we can choose to only take the free conducting electrons that are not bound to a nucleus into account and put ω_0 to zero. The polarization $\mathbf{P}$ of the metal can be written [30]:

$$\mathbf{P} = N\mathbf{p} = -Ne\mathbf{x} = -\frac{\frac{Ne^2}{m}}{\omega^2 + i\omega\gamma}\mathbf{E}$$

where N is the electron density of the metal. The electric flux density $\mathbf{D}$ is [30]:

$$\mathbf{D}(\omega) = \epsilon_0\mathbf{E} + \mathbf{P}(\omega) = \epsilon_m(\omega)\mathbf{E}$$

where $\epsilon_0 \approx 8,854 \cdot 10^{-12}$ F/m is the permittivity of free space. From the expressions above the permittivity of the metal, $\epsilon_m(\omega)$, can be derived.

$$\epsilon_m(\omega) = \epsilon_0 - \frac{\frac{Ne^2}{m}}{\omega^2 + i\omega\gamma} = \epsilon_0\left(1 - \frac{\omega_p^2}{\omega^2 + i\omega\gamma}\right)$$

We use the plasma frequency of the metal defined as $\omega_p = \sqrt{\frac{Ne^2}{\epsilon_0 m}}$. The relative permittivity, also called the dielectric function, can then also be expressed as a function of frequency:

$$\varepsilon_{mrel}(\omega) = \frac{\epsilon_m(\omega)}{\epsilon_0} = 1 - \frac{\omega_p^2}{\omega^2 + i\omega\gamma} \tag{5.1}$$

This way of modeling a metal is referred to as the Drude model [31].

In the following formulas and derivations I will use the relative permittivity ε_{rel} rather than the absolute permittivity ϵ. For simplicity I will from now on drop the index and write only ε when I refer to the relative permittivity.

In the Drude model we choose to disregard the effects of any bound charges in the metal. In most cases this is a very good approximation. When comparing to experimental data for the permittivity of metals the Drude model is reasonably accurate above 400 nm for silver, above 650 nm for gold and all the way up to ultraviolet for alkali metals [27]. For higher energies bound electrons in silver and gold will get excited and the Drude model is not a good approximation. The derivation of the dielectric constant for a Lorentz material and the Drude model can be found in most electromagnetic wave propagation textbooks, including [32], [30] and [27].

5.3 Electromagnetic wave propagation in metals

Using the Drude model defined in equation 5.1 we can write the propagation constant of an EM-wave in a metal as [27]:

$$k_m = \sqrt{\varepsilon_m(\omega)}\frac{\omega}{c_0} = \sqrt{1 - \frac{\omega_p^2}{\omega^2 + i\omega\gamma}}\frac{\omega}{c_0}$$

To get a qualitative feeling for how propagation in the metal depends on frequency we can simplify the expression above by ignoring losses caused by collisions and setting $\gamma = 0$. We then treat the metal as a lossless electron plasma and the wave vector has the simple form:

$$k_m \approx \frac{1}{c_0}\sqrt{\omega^2 - \omega_p^2}$$

We can see that k is imaginary for $\omega < \omega_p$, and no EM-waves below the plasma frequency can propagate in the metal. At the plasma frequency the free electrons inside the metal oscillate collectively, creating longitudal electromagnetic waves called bulk plasmons. Above the plasma frequency the plasma is transparent for EM-waves. In practice visible wavelengths will be absorbed very quickly in the metal, and interband transitions in the noble metals cause the Drude model to fail for high frequencies, [27].

5.4 Surface waves on a dielectric-metal interface

Although no EM-waves below the plasma frequency can propagate inside a metal, there can be surface waves propagating along the metal surface. An electromagnetic wave confined to the surface of a metal is called a *surface plasmon polariton*, or SPP for short. The wave is sustained by *surface plasmons*, oscillations in the conducting electrons on the metal surface, [27].

In appendix 1 it is shown that a surface plasmon polariton, or SPP for short, is a TM-polarized electromagnetic wave confined to an interface. It is also shown that an SPP-mode is only supported if the real part of the permittivity has different signs on opposite sides of the interface:

$$\mathrm{Re}\varepsilon_1 > 0$$

$$\mathrm{Re}\varepsilon_2 < 0$$

where 1 and 2 refers to the different materials at each side of the interface. This typically applies to an interface between a metal an a dielectric.

The electromagnetic fields of an SPP decay exponentially perpendicular to the interface with a rate determined by material parameters. The wavelength of a surface plasmon polariton can be considerably shorter than the wavelength in vacuum for the same frequency. This leads to a high confinement of the electric field, and very high field strengths can be obtained.

Unfortunately surface plasmon polaritons suffer from high attenuation coefficients and can't propagate more than some tens of micrometers before they are absorbed in the metal. There are ways to reduce the dissipation and increase the propagation length, but there is always a trade off between high field confinement and low attenuation.

Surface plasmon polaritons is the basic physical mechanism behind optical antennas and metallic structures for manipulation of light. They will be investigated in more detail in the following chapter.

Chapter 6

Surface plasmon polaritons on a semi-infinite flat surface

In this chapter we will consider the simplest case of a surface plasmon polariton propagating along a semi-infinite flat interface between a metal and a dielectric of some kind. Coupling mechanisms between an SPP and a photon will be investigated as well as the wavelength and lifetime of the SPP.

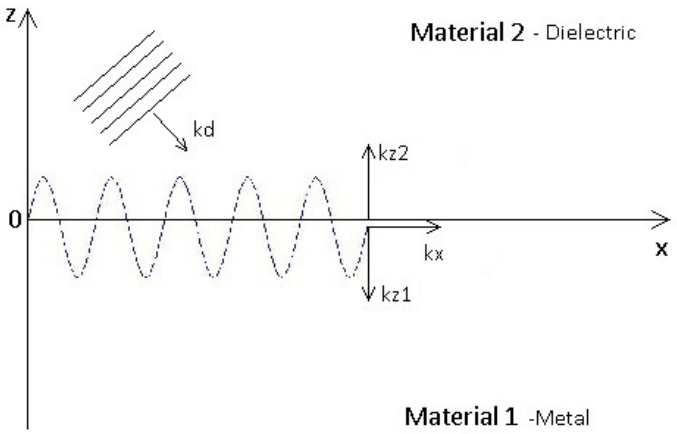

Figure 6.1: Geometry used in this chapter: An SPP propagating along the x-axis.

We choose to place an interface between two materials at $z = 0$ in a Cartesian coordinate system and assume that all light propagates in the x-z-plane. The SPP propagates along the interface in the x-direction, as shown in figure 6.1. The z-components of the SPP-wave vector is imaginary in both materials so that the fields decay exponentially away from the surface.

6.1 Dispersion relation

Following the geometry outlined above we have a surface plasmon polariton propagating in the x-direction along an interface between a metal and a dielectric at $z = 0$. The wavenumber of the SPP in each material, k_i with $i = 1$ for the metal or $i = 2$ for the dielectric, can be written in

terms of the wave number in vacuum, k_0, or in terms of it's x- and z-components:

$$k_i^2 = \varepsilon_i k_0^2 = k_{xi}^2 + k_{zi}^2$$

If we require the fields parallel to the surface to be continuous across the surface we get the following condition, (see appendix A for details):

$$\frac{k_{z2}}{k_{z1}} = -\frac{\varepsilon_2}{\varepsilon_1}$$

The wave vectors pointing along the surface are also continuous across the surface, $k_{x1} = k_{x2}$. This yields a dispersion relation for a surface plasmon polariton [30], [27]:

$$k_{sp} = k_{x1} = k_{x2} = k_0 \sqrt{\frac{\varepsilon_1 \varepsilon_2}{\varepsilon_1 + \varepsilon_2}} \tag{6.1}$$

This relation can be seen in figure 6.2 where a Drude model has been used. In the same figure the light line in the dielectric medium is shown, $k_d = \frac{2\pi\omega n_2}{c_0}$, where $n_2 = \sqrt{\varepsilon_2}$ is the refractive index in the dielectric and c_0 is the speed of light in vacuum. k_d is real and hence the component along the surface can never be greater than k_d itself;

$$k_{xd} \leq k_d$$

It can be seen in the figure that for each frequency $\omega \neq 0$ $k_d < k_{sp}$ and hence also $k_{xd} < k_{sp}$. The wave vector along the x-axis of the dielectric mode can never be matched to the wave vector of the surface plasmon polariton.

$k_{sp} > k_d$ is equivalent with saying that the SPP always has a shorter wavelength than light propagating in the dielectric, $\lambda_{sp} < \lambda_d$. At the surface plasmon resonance $\omega_{sp} = \frac{\omega_p}{\sqrt{2}}$ the SPP wavelength will go to zero, as can be seen in figure 6.2(b). This together with the rapid decay perpendicular to the interface gives the SPP a very localized field distribution with very high field strengths as a result.

6.2 Coupling to a surface plasmon polariton mode

As can be seen in figure 6.2 in the previous section it is not possible to couple an incoming EM-wave directly to a surface plasmon polariton mode, since $k_{sp} > k_d \geq k_{xd}$. This can be easily realized by considering an incoming plane wave from the dielectric as in figure 6.3. Depending on the angle of incidence the effective wavelength along the surface can be equal to or larger than the wavelength of the plane wave, but it is not possible to match a surface wave with a shorter wavelength.

One way to achieve phase matching between an incoming wave and an SPP is to use frustrated total internal reflection from a denser material, as in figure 6.4. By for example letting the light be incident from a prism on one side of a metal film a surface plasmon polariton can be excited on the other side of the film. This will cause total internal reflection at the prism-metal interface, but as long as the metal film is thin enough the evanescent field from the prism can tunnel through the barrier and excite an SPP on the opposite metal-dielectric interface [30].

Another way of achieving phase matching between an incident field and an SPP on a flat surface is by using a grating. The grating can provide the incoming field with additional momentum and increase the wavenumber. A rough surface can in some sense be viewed as a randomized grating. An incoming wave can excite an SPP along a rough surface directly, but the SPP will also be scattered by sharp edges along the surface.

6.3 Decay rate of a surface plasmon polariton

The decay rate of an SPP mode depends on the material parameters of the surrounding media as well as the shape of the surface. The imaginary part of the wave number $k_{sp} = k_x$ determines the

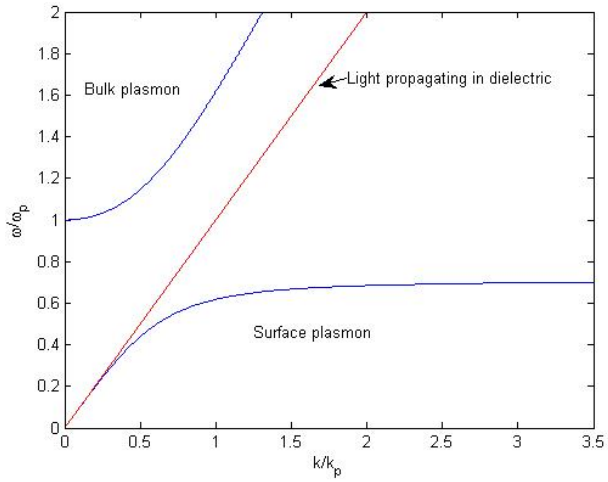

(a)

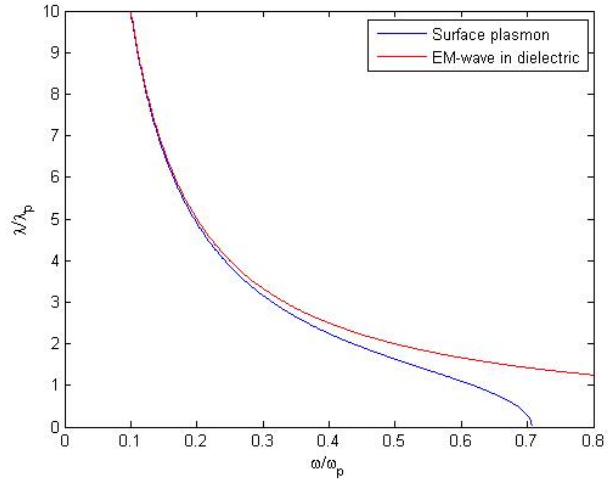

(b)

Figure 6.2: Plasmon dispersion relation in terms of (a) wavenumber and (b) wavelength.

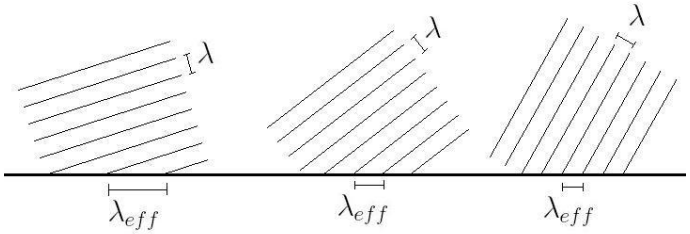

Figure 6.3: A plane wave reaching a surface. The effective wavelength along the surface is always bigger than on equal to the wavelength of the plane wave.

decay rate of the mode.

$$E \propto e^{ik_{sp}x} = e^{iRek_{sp}x} e^{-Imk_{sp}x}$$

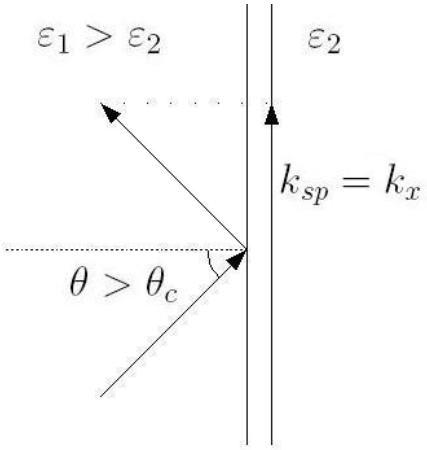

Figure 6.4: The evanescent field from a denser material on one side of a metal film can excite an SPP on the other side.

For a semi-infinite metal film the dispersion relation was found in 6.1, repeated here for clarity:

$$k_{sp} = k_0 \sqrt{\frac{\varepsilon_1 \varepsilon_2}{\varepsilon_1 + \varepsilon_2}}$$

As an example we look at an interface between silver and air using the experimental value $\varepsilon_m \approx -16 + 0.5i$ for silver at 600 nm [27].

$$k_{sp} \approx 11 + 0.011i \ /\mu\text{m}$$

The effective propagation length is:

$$\delta = \frac{1}{\text{Im}(k_{sp})}) \approx 91\mu\text{m}$$

A surface plasmon polariton will propagate less than 100 μm along a flat surface if no other losses than absorption are taken into account. A real surface is never completely smooth and there will be scattering in addition to absorption.

Writing $\varepsilon_m = \text{Re}\varepsilon_m + i\text{Im}\varepsilon_m$ and expanding k_{sp} to first order in $\text{Im}\varepsilon_m$ we can write [30]:

$$\text{Im}(k_{sp}) \approx -k_0 \left(\frac{\varepsilon_d \text{Re}(\varepsilon_m)}{\text{Re}(\varepsilon_m) - \varepsilon_d} \right)^{3/2} \frac{\text{Im}(\varepsilon_m)}{2\text{Re}(\varepsilon_m)^2}$$

We can see that $\text{Im}(k_{sp})$ is proportional to k_0 and hence the propagations length $\delta \propto \frac{1}{k_0}$ to first order. The propagation length decreases for higher frequencies. It is however important to keep in mind that the Drude model is not valid for wavelengths shorter than 400 nm in silver.

Chapter 7

Localized surface plasmons

Propagating surface plasmon polaritons were investigated in the previous chapter. We assumed a semi-infinite interface between a metal and an insulator and saw that the surface plasmon polariton is a TM-polarized EM-mode that can not be excited directly by an incident plane wave.

In this chapter another type of surface plasmon excitation will be investigated, namely localized surface plasmons. The free electrons on the surface of a small metallic structure will oscillate in a time-harmonic electric field. The curvature of the surface will affect the restoring force on the electrons. At resonance there is a large field enhancement close to the metal structure due to the oscillating charges. A localized surface plasmon is a non-propagating excitation that can couple directly to incident light.

The interaction between light and structures much smaller than the wavelength can be treated using quasi-static theory. The special case of a metal sphere will be treated in depth since it is analytically solvable and provides a good example.

7.1 A small sphere in an electric field

7.1.1 Quasi-static approximation

We consider a small sphere with radius much smaller than the wavelength of the incident light, $a << \lambda$, in a static electric field.

$$\mathbf{E}_0 = E_0\hat{\mathbf{z}}$$

The sphere has a complex relative permittivity $\varepsilon_m(\omega)$ that can be explicitly stated using the Drude model as in equation 5.1 in chapter 5.1. The surrounding medium is assumed to be non-absorbing with permittivity ε_d. Applying suitable boundary conditions for the sphere the problem can be solved and the resulting electric fields inside and outside the sphere respectively are [33] [27]:

$$\mathbf{E}_{in}(\mathbf{r}) = \frac{3\varepsilon_d}{\varepsilon_m(\omega) + 2\varepsilon_d}\mathbf{E}_0 \tag{7.1}$$

$$\mathbf{E}_{out}(\mathbf{r}) = \mathbf{E}_0 + \frac{3\mathbf{n}(\mathbf{n}\cdot\mathbf{p}) - \mathbf{p}}{4\pi\varepsilon_0\varepsilon_d r^3} \tag{7.2}$$

where $\mathbf{n} = \frac{\mathbf{r}}{|\mathbf{r}|}$ is a unit vector in the direction of the point of interest and $\mathbf{p}$ is the dipole moment of the sphere:

$$\mathbf{p} = 4\pi\varepsilon_0\varepsilon_d a^3 \frac{\varepsilon_m(\omega) - \varepsilon_d}{\varepsilon_m(\omega) + 2\varepsilon_d}\mathbf{E}_0 = \varepsilon_0\varepsilon_d\alpha\mathbf{E}_0$$

Here we define the polarizability of the sphere, $\alpha = 4\pi a^3 \frac{\varepsilon_m(\omega)-\varepsilon_d}{\varepsilon_m(\omega)+2\varepsilon_d}$. The field outside the metal sphere is in this approximation a superposition of the incoming field and the field from a point dipole.

A resonance occurs when the polarizability has a maximum, hence when $\varepsilon_m(\omega) + 2\varepsilon_d$ is close to zero. Assuming $\mathrm{Im}(\varepsilon_m)$ is small, the resonance condition is:

$$\mathrm{Re}(\varepsilon_m(\omega)) = -2\varepsilon_d \tag{7.3}$$

This is called the Fröhlich condition. Note that in this approximation the size of the sphere does not influence the resonance frequency.

When applying an oscillating electric field to the metal sphere the dipole moment of the sphere will also oscillate and make the sphere radiate. The incoming wave is scattered by the sphere. The radiated fields from a dipole are $\mathbf{H}(t) = \mathbf{H}e^{-i\omega t}$ and $\mathbf{E}(t) = \mathbf{E}e^{-i\omega t}$, where $\mathbf{E}$ and $\mathbf{H}$ are [33]:

$$\mathbf{H} = \frac{ck^2}{4\pi}(\mathbf{n}\times\mathbf{p})\frac{e^{ikr}}{r}\left(1-\frac{1}{ikr}\right)$$

$$\mathbf{E} = \frac{e^{ikr}}{4\pi\varepsilon_0\varepsilon_d}\left(\frac{k^2}{r}(\mathbf{n}\times\mathbf{p})\times\mathbf{n} + (3\mathbf{n}(\mathbf{n}\cdot\mathbf{p})-\mathbf{p})\left(\frac{1}{r^3}-\frac{ik}{r^2}\right)\right)$$

k is here the wave number in the surrounding medium. Close to the dipole we can assume $kr << 1$ and we only need to take terms proportional to $\frac{1}{r^3}$ into account. Then the electric field is reduced to:

$$\mathbf{E}_{near} = \frac{3\mathbf{n}(\mathbf{n}\cdot\mathbf{p})-\mathbf{p}}{4\pi\varepsilon_0\varepsilon_d r^3}$$

which is exactly what we got above using the quasi-static approximation.

The imaginary part of the polarizability $\mathrm{Im}(\alpha)$ accounts for absorption losses in the metal. The absorption cross section is proportional to the volume of the sphere while the scattering cross section scales as the volume squared [27].

$$C_{abs} \propto a^3$$

$$C_{scat} \propto a^6$$

For very small particles absorption will dominate over scattering. Both cross sections are resonantly enhanced when the Fröhlich condition is satisfied.

Assuming that the sphere is made out of silver with $\omega_p \approx 1.4 \cdot 10^{16}$ rad/s [29] and surrounded by air the Fröhlich condition 7.3 gives the resonance frequency:

$$\omega_{res} = \frac{\omega_p}{\sqrt{3}} \approx 8 \cdot 10^{15}\mathrm{rad/s}$$

$$\lambda_0 \approx 233\mathrm{nm}$$

λ_0 is the resonant free space wavelength.

The relative permittivity of the surrounding medium will influence the resonance frequency of the metal particle. Assuming an excitation wavelength of 600 nm (in vacuum) and using the relative permittivity of silver at this wavelength $\varepsilon_m = -16+0.5i$ [27], we get a resonance if the surrounding medium has a relative permittivity of

$$\varepsilon_d = -\frac{\mathrm{Re}(\varepsilon_m)}{2} = 8$$

The quasi-static approximation used here is strictly valid only for a vanishing particle diameter when the sphere acts as a perfect point dipole. It is however approximately valid for diameters smaller than the wavelength of the incident light. In this case it is assumed to be valid up to a particle diameter of about 100 nm.

Some features of localized surface plasmons are not captured by this description, as for example radiative damping and size-dependence of the resonance frequency.

7.1.2 Second order expansion

There are two regimes where the quasi-static approximation breaks down: for particles smaller than the mean free path of the oscillating electrons and for particles big enough for retardation effects to be important. I will only focus on the case of larger particles, since I won't consider any structure smaller than 10 nm within this thesis.

Mie theory gives a rigorous treatment of scattering and absorption by a sphere using an electrodynamic approach. I will satisfy with a second order expansion of the polarizability α, [27]:

$$\alpha = V \frac{1 - 0.1(\varepsilon_m + \varepsilon_d)x^2 + O(x^4)}{(1/3 + \frac{\varepsilon_d}{\varepsilon_m - \varepsilon_d}) - 1/30(\varepsilon_m + 10\varepsilon_d)x^2 - i\frac{4\pi^2\varepsilon_d^{3/2}}{3}\frac{V}{\lambda_0^3} + O(x^4)} \tag{7.4}$$

$$x = \frac{\pi a}{\lambda_0}$$

x is a size-parameter, depending on the radius a and the free space wavelength λ_0, and V is the volume of the sphere.

The terms quadratic in x accounts for retardation effects in the field outside and inside the sphere. For a Drude-metal they lead to a red shift of the resonance frequency for increasing particle size.

The imaginary term in the denominator is due to radiation damping. A localized plasmon mode can decay directly into a photon and this will lead to a weakening of the resonance as well as broadening. The term is proportional to the volume of the sphere and thus increases rapidly with particle size.

To get a better feeling for how the second order expansion will affect the polarizability we can compare with the polarizability given by the quasi static approximation, α_{qs}, for a wavelength of 600 nm and a silver sphere of diameter 50 nm surrounded by air.

$$\alpha_{qs} \approx (2.38 + 0.015i) \cdot 10^{-22}\text{C/m}$$
$$\alpha \approx (2.41 + 0.05i) \cdot 10^{-22}\text{C/m}$$

The difference is not very big, especially the real part of the polarizability is almost the same in the two cases. The imaginary part is bigger for the second order expansion since we now take radiation damping into account.

7.2 Lifetime of a localized surface plasmon

A localized surface plasmon has a limited lifetime due to the damping processes mentioned above. The plasmon can be modeled in a simplified way as a two-level system in a thermal reservoir. Taking all dephasing processes into account and assuming a Lorentzian line shape we can define a total dephasing time, T, in terms of the plasmon resonance linewidth in frequency, $\Delta\nu$, and angular frequency, $\Delta\omega$, [28]:

$$T = \frac{1}{\pi\Delta\nu} = \frac{2}{\Delta\omega}$$

There are two contributions to the dephasing time T, a lifetime due to damping, T_1, and a pure dephasing time limited by elastic collisions, T_2. In normal circumstances the absorption and radiation probabilities are much higher than the collision frequency, so that $T_1 << T_2$ and $T \approx T_1$.

For small gold and silver spheres experiments show that T is in the order of a few femtoseconds, [27]. The dephasing time depends on the shape and size of the particle as well as the surrounding media. Smaller particles will in general have longer lifetimes, and a prolate shape will increase the lifetime compared to a spherical shape as was shown by Sönnichsen et al, [34]. In the same study the longest obtained lifetime for gold nano rods was 18 fs. The lifetime can be increased by

choosing silver instead of gold because of the lower absorption, but still the dephasing time will probably be limited to tens of femtoseconds.

7.3 Plasmonic antennas

Optical antennas are used in a variety of applications, mainly for enhanced emission and sensing. The localized plasmon resonance of a small metal structure depends on the properties of the surrounding medium. This can be used to detect small changes of refractive index for example within biosensing, [35]. Plasmonic antennas have received a lot of attention in the context of surface enhanced Raman spectroscopy, SERS. SERS enhancement factors as high as 10^{14} are obtained and with clever designs even higher factors are possible, [36]. The enhancement is partly due to an enhanced field strength at hot spots close to metallic particles.

The high field enhancement close to a plasmonic antenna is due to two effects. Firstly, the localized surface plasmon resonance will give rise to strong near fields and hot spots in small gaps between particles. Secondly, there is a well known phenomenon from antenna theory called the *lightning rod effect*. It means that the electric field is high at sharp edges due to a crowding of the field lines. The lightning rod effect is a pure geometrical effect taken advantage of when designing antennas for high field enhancement.

The Bowtie antenna is a variant of a dipole antenna, built out of two triangular antenna elements facing each other tip to tip, as shown in figure 7.1. It is a widely used antenna, for example to receive high frequency radio waves. The sharp edges in the center of the bowtie antenna creates a small focus and high field strength in the gap between the antenna elements.

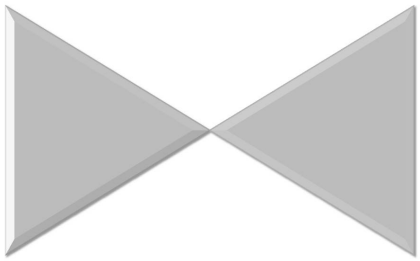

Figure 7.1: A bowtie antenna.

In 1997 Grober et al. [37] showed that microwaves can be focused down below the diffraction limit with high field strengths as a result using a bowtie antenna. In the same article they propose to scale down the antenna to optical wavelengths. Since then the bowtie antenna has been a popular choice at optical wavelengths and studied theoretically and in experiments, [38] [39].

7.4 A note on non-locality

When considering light-matter interaction a semi classical theory is often used. Light is treated as a classical EM-wave while atoms are treated using quantum mechanics. In macroscopic systems, like big chunks of matter, we assign certain properties to each material. We assume that an incident electric field induces a response in the material determined by material parameters like for example the permittivity. The response is assumed to be local so that the electric field at each point induces a polarization in this point only. In this way we only consider averaged quantities and don't have to take each single atom into account. The interaction between different regions are modeled with suitable boundary conditions. This does not work well for smaller systems when the interaction

between induced dipoles at different locations becomes important. This non-local response can be seen as a consequence of quantum mechanics. If the spatial wave function of a collection of atoms is coherent, a force applied at one point must affect the wave function in all points.

A full treatment of this problem would require a quantization of both matter and the electric field. It is possible to include a non-local optical response in a semi classical theory, but this is often not done in basic electromagnetic wave propagation textbooks or in commercial computer software. In most applications a local approximation works very well.

Examples of when a local approximation fails is for very small structures or gaps as well as for very sharp edges. A typical plasmonic antenna has both sharp edges and a very small gap between two antenna elements. When putting two small metal particles close to each other they strongly influence one another. This will change the local fields and also shift the plasmon resonances of the metal structures, [40].

This effect is not taken into account in this work. By keeping a minimum distance of 2 nm between the antenna elements and by rounding off sharp edges to a minimum radius of curvature of 5 nm the effects of non-local response are assumed to be negligible.

Chapter 8

Modeling using COMSOL Multiphysics®

To simulate an antenna placed at the surface of a crystal I use COMSOL Multiphysics®, a commercial finite element simulator used within many different fields. Comsol was developed in the early 90's under the name FEMLAB®. Today Comsol Multiphysics is a big family of software with several add-on modules specialized for applications like structural mechanics, heat transfer and electromagnetic wave propagation. The multiphysics capability means that several different kinds of physical phenomena can be simulated and combined. As an example the result from an electromagnetic wave propagation simulation can be used as input data for a heat transfer simulation. I have used the RF-module of Comsol which suits well for applications within photonics and electromagnetic wave propagation.

Using Comsol it is possible to define arbitrary geometries and shapes with different material parameters. It is also possible to import a geometry from a CAD-model. The program makes use of the finite element method to solve the given differential equations within the defined geometry.

8.1 The finite element method

The finite element method, FEM, is a numerical method of solving differential equations in one-, two- or three-dimensional geometries. Instead of finding an approximate solution in the entire region of interest the region is split up into finite elements and an approximate solution is found for each element. The approximation made for each element can be rather simple, for example that the variable of interest changes linearly within the element. Each element has a number of nodal points, usually placed at the boundary. If the solution is known in the nodal points, the approximate solution for the entire element is obtained simply by interpolating the nodal points. The continuous problem is thus transformed to the discrete problem of finding the solution to the differential equation in the nodal points.

The number of unknowns is equal to the number of nodal points in the defined mesh of finite elements. A finer mesh with a larger number of nodal points will give a more accurate solution. In general the number of nodes is very large. Especially for three-dimensional problems the number of elements grow fast with the size of the geometry. The finite element method is dependent on effective computers to store big matrices and solve big equation systems.

The finite element method can be used to solve any differential equation in an arbitrary geometry. It is one of the most powerful numerical methods available and used within all areas of engineering. For a more complete description of FEM I recommend [42].

8.2 Model

The RF-module of Comsol Multiphysics is suitable for modeling electromagnetic wave propagation. The size of the geometry is in this case on the limit where a quasi-static model might be enough, but in this case the electromagnetic wave propagation application mode will be used, which is based on the full Maxwell equations. A quasi-static approximation will not describe some of the properties of localized surface plasmons in a satisfactory way, as was mentioned in connection with the theoretical treatment of a small metallic sphere in chapter 6.

A scattered harmonic propagation analyses is used. Harmonic propagation means that all waves have a harmonic time dependence, which gives the possibility to use a complex field formulation. Doing that it's not necessary to solve the equations for each time step.

A scattered field formulation means that the incoming field is pre-defined in the entire volume and the scattered field is solved for. This is particularly good when using perfectly matched layers, PMLs, which will be discussed in the next section. In this way the incident field is defined in the entire volume outside the PML-regions and will not be affected by the absorbing PMLs at all.

Using a scattered harmonic propagation analyses the wave equation for the scattered electric field is solved.

$$\nabla \times \left(\frac{1}{\mu} \nabla \times \mathbf{E}_{sc} \right) - \varepsilon k_0^2 \mathbf{E}_{sc} = 0$$

$$\mathbf{E} = \mathbf{E}_{in} + \mathbf{E}_{sc}$$

The incident electric field is defined as:

$$\mathbf{E}_{in} = \hat{e}_x e^{-1.8ik_0 y} e^{-1.5k_0 z}$$

The field is propagating along the y-axis and is polarized along the length of the antenna in the x-direction. The field decays exponentially in the z-direction towards the antenna and crystal surface.

$k_0 = \frac{2\pi}{\lambda_0}$ is the wave number in vacuum. $1.8k_0 = k_y$ is the y-component of the wave vector and $-i1.5k_0 = k_z$ is the z-component of the wave vector. The wave numbers have been chosen by assuming a plane wave propagating in the y-direction in a glass of refractive index 1.8 just above the modeled volume. The wave number in this glass is then: $k_{yglass} = 1.8k_0$. Since the component of the wave vector parallel to the surface is continuous across the surface:

$$k_{yglass} = k_y = 1.8k_0$$

and also

$$k_0^2 = k_y^2 + k_z^2 \rightarrow k_z = -\sqrt{(1 - 1.8^2)}k_0 = -i1.5k_0$$

The negative square root is chosen since the field is exponentially decaying.

The situation is shown in figure 8.1, where the electric field is perpendicular to the plane of the image. The glass is not part of the Comsol model, but the evanescent field is defined directly as input data.

Normal silica glass has a refractive index of about 1.5. The reason for using a refractive index of 1.8 and not 1.5 is to avoid a propagating wave inside the crystal. If light was incident from a glass with refractive index 1.5 the pre-defined field E_{in} would not be evanescent inside the crystal. This will be discussed more in chapter 12.

The chosen field is not based on the situation with a toroidal microresonator but is a very simplified evanescent field with an amplitude equal to one at the surface of the geometry. The specific amplitude of the field is not important since I will only consider the enhancement of the field relative to a reference based on the same model.

The free space wavelength used is $\lambda_0 = 600$ nm.

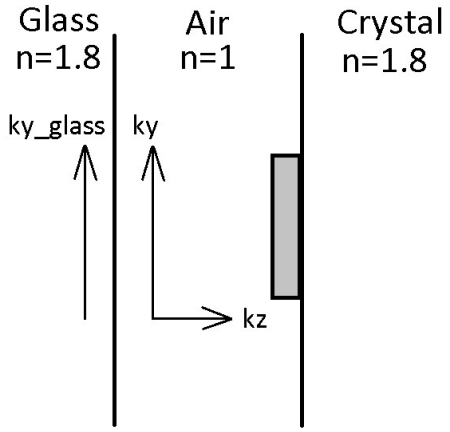

Figure 8.1: An evanescent wave with an imaginary component k_z is incident on the antenna.

8.3 Geometry

To solve the differential equations given above we need to define a geometry with suitable material parameters and boundary conditions. The convergence and error of a simulation depends very much on the geometry so it might be worth taking some time to think about the situation we want to solve.

The geometry consists of a block representing the crystal surface. On top of the block an antenna structure is placed. The crystal and the antenna are contained in a second bigger block of air. This block is the volume where the equations will be solved. The volume is surrounded by PML-regions which will be discussed more in connection with boundary conditions. There is also a smaller block surrounding the antenna. This block has no physical meaning, it has the same material parameters as the surrounding material, but is there to make it possible to define a different mesh gradient close to the antenna. This will be discussed more in connection with meshing.

The antenna has it's length along the x-axis. The z-axis is pointing in the direction from air to the antenna and down into the crystal.

The geometry can be seen in figure 8.2. The dimensions and material parameters for my model are given below.

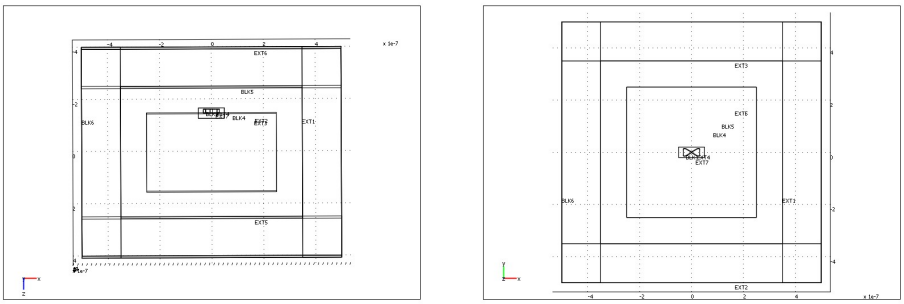

(a) (b)

Figure 8.2: Geometry seen (a) from the side in the x-z-plane and (b) from the top in the x-y-plane.

Volume with air:

Length along x-axis	700 nm
Width along y-axis	700 nm
Height along z-axis	500 nm
Center point	(0,0,0)

$\varepsilon_{air} = 1$

Crystal:

Length along x-axis	500 nm
Width along y-axis	500 nm
Height along z-axis	300 nm
Center point	(0,0,0)

$$\varepsilon_{crystal} = \begin{pmatrix} 3.27 & 0 & 0 \\ 0 & 3.19 & 0 \\ 0 & 0 & 3.20 \end{pmatrix}$$

This data is for the Y_2SiO_5 host crystal, [41]. In this case the crystal is oriented with the optic axis along the x-axis.

Metal structures:

Varying sizes and shapes.

$\varepsilon_m = -16 - 0.5i$

The value is taken from experimental data, but is consistent with the Drude model, [27].

One important thing to note is that Comsol uses the opposite sign convention from what I have done in this thesis, and hence the imaginary part of the permittivity of a metal has the opposite sign from what I have used in previous chapters and from what is given in [27].

8.4 Boundary conditions

One of the biggest challenges when modeling wave propagation is to find suitable boundary conditions. We want light to propagate out from our volume without being reflected back. This might seem like an easy thing to do, but when formulating this as a boundary condition for a differential equation we need some information about the field at the boundaries. Comsol offers two different boundary conditions for this situation.

The scattering boundary condition will be completely transparent and non-reflecting for plane waves. This is suitable for an incident plane wave if the volume is big enough so that scattering occurring inside the volume does not affect the field at the boundaries too much. If the wavefronts are not planar at the boundary they will be at least partly reflected.

The matched boundary condition is completely transparent and non-reflecting for guided modes with a pre-defined wave vector. This suits well for modeling of waveguides, but not so well for scattered waves.

The scattering boundary condition caused a lot of reflections in this model. Since lack of computer memory was one of the major limitations for the model I didn't wan't to increase the volume too much. There is a third option when both of the above mentioned boundary conditions fail; namely to use perfectly matched layers, PML's. PML's are impedance matched absorbing layers placed at the boundary of the volume. They will absorb outgoing radiation before it is reflected back into the volume. By combining PML's with a scattering boundary condition reflections can be minimized for arbitrary wavefronts and wave vectors. A PML is not simply a special material placed at the boundary. No physical material can have both a perfectly matched impedance to the interior of the volume and a high absorption compared to the interior. Mathematically a PML-region is modeled

by a special coordinate transformation. The exact mathematical formulation of the PML-regions is outside the scope of this thesis.

8.5 Mesh

To solve the wave equation in the geometry defined above we need to create an element mesh. Linear triangular elements are the simplest possible elements in a 3D-geometry. They are flexible and easy to fit into sharp edges and small structures.

Smaller elements give a smaller error in the approximation. Small details in the geometry need a finer mesh than big structures. The element size is limited by the accessible RAM memory of the computer.

According to the Nyquist theorem we need at least two linear elements per wavelength to model the field. The Comsol Multiphysics users guide recommends 10 elements per wavelength, and an element size of about half the size of the smallest structure in the model.

A problem with this model is that the size of the entire block is rather large, about 700 nm in each direction, compared to the smallest structures which for the antennas are just a few nanometers. Because of lack of memory a fine mesh can't be used in the entire geometry but we need a very fine mesh close to the antenna. The solution is to use different mesh sizes in different regions. It is also possible to define a gradient of the mesh size, so that the elements get gradually bigger away from the antenna. In the outer parts of the volume the mesh can be rather coarse since we're not interested in the fields far away from the antenna.

A fine mesh is defined in the metal structure. In most cases 2 nm long mesh elements are used inside the antenna which is the smallest possible size with the accessible 6 GB of RAM memory. In the small box surrounding the antenna, where we are interested in calculating the fields, a small gradient of the element size is used. A gradient of 1.1 means that each mesh element will be 1.1 times bigger than the previous one, starting from the antenna. In the rest of the volume a larger gradient of 1.3 is defined. If an even larger gradient is used the solution does not converge. Part of a two-dimensional version of the mesh can be seen in figure 8.3.

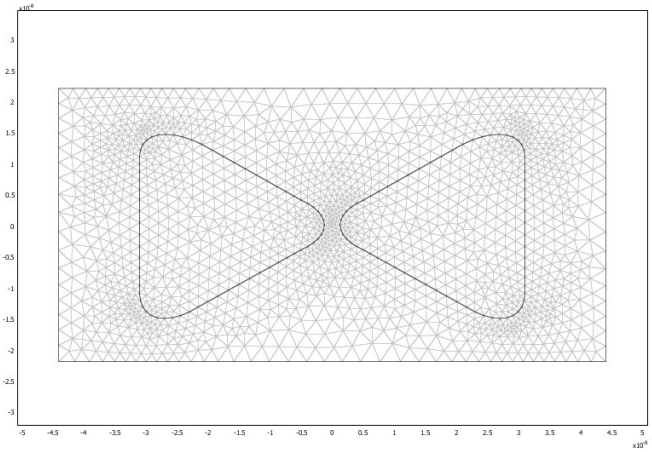

Figure 8.3: Mesh surrounding a bowtie antenna.

To check how the mesh size will affect the result of a simulation a bowtie antenna is simulated with several different mesh sizes inside the antenna. In figure 8.4 the field strength between the antenna elements on the surface of the crystal is plotted as a function of mesh size.

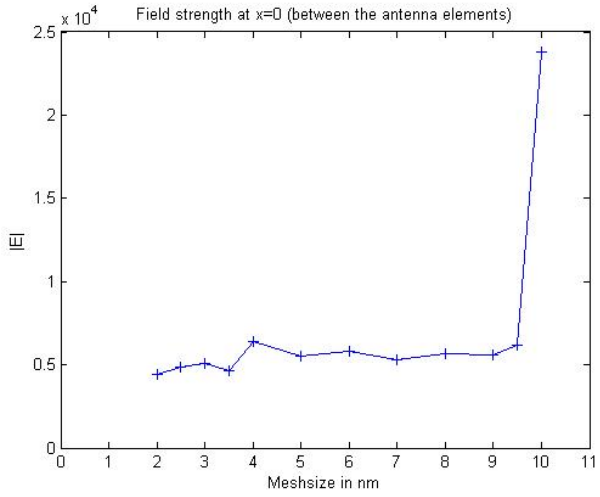

Figure 8.4: Electric field as a function of mesh size.

The result does not vary very much with mesh size, except for elements as big as 10 nm. For elements bigger than 10 nm the solution does not converge. The distance between the antenna elements are in this case 5 nm. For a maximum mesh size of 5 nm or bigger there is at least one mesh element in the gap between the antenna elements. For a mesh size of 2.5 - 4 nm there will be at least two elements across the gap and for a 1.7 - 2.5 nm mesh there will at least three elements. The field decays rapidly away from the sharp tips of the bowtie and the number of elements in the gap as well as the location of the nodes can have a big influence on the field in the gap. From 8.4 it seems like we need an elements size of 3.5 nm or below.

I used the GMRES iterative solver and allowed an error of $1 \cdot 10^{-6}$ V/m.

Chapter 9

Comparison between a simulation and theory

To evaluate the model described in the previous chapter a small sphere is simulated using Comsol Multiphysics. The result from the simulation is compared to a theoretical treatment using a second order expansion of the polarizability as described in chapter 7. The theoretical equations are put into a MatLab script to generate plots similar to those given by Comsol.

9.1 Models

For the numerical simulation the analysis mode, incident field and boundary conditions described in the previous chapter are used. The geometry consists of a silver sphere surrounded by air, positioned as in figure 9.1. The small box around the sphere is only for meshing purposes and has the same material parameters as the surroundings. The sphere has a diameter of 50 nm. The mesh elements have a maximum size of 3 nm inside the sphere. The size of the mesh elements increase with a gradient of 1.1 in the small box surrounding the sphere and with a gradient of 1.3 in the rest of the volume.

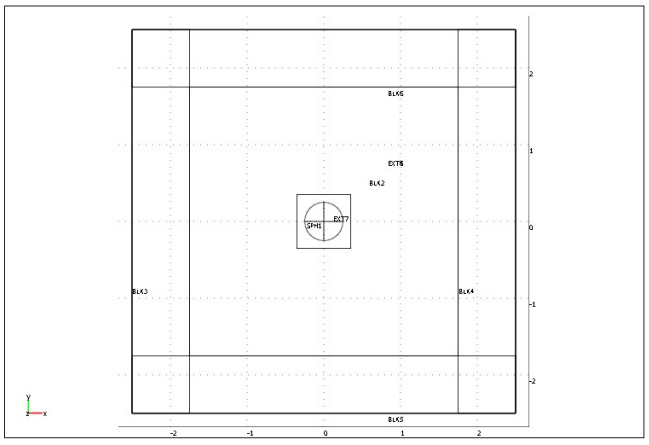

Figure 9.1: Geometry used for simulation.

The theoretical calculation is done with the help of MatLab using the same incident field and

material parameters as for the FEM simulation. The fields inside and outside the metal sphere are given by equations 7.1 and 7.2. The polarization of the sphere is:

$$\mathbf{p} = \varepsilon_0 \varepsilon_d \alpha \mathbf{E}_0$$

where the polarizability α is given by the second order expansion in equation 7.4.

9.2 Results

The norm of the electric field is shown in figure 9.2. Figure 9.2(a), generated by using a theoretical approximation, has a periodic background of an electric field propagating in the y-direction. Even though the free space wavelength of the incident field is 600 nm the field has a wavelength of 333 nm in the y-direction, since it is an evanescent field. The wave vector, k_0, then has an imaginary component in the z-direction which will contribute to the total length, $k_0^2 = k_x^2 + k_z^2$.

The background looks different for the Comsol simulation, 9.2(b). This is due to reflections at the boundaries which have a clearly visible effect even though PML's are used.

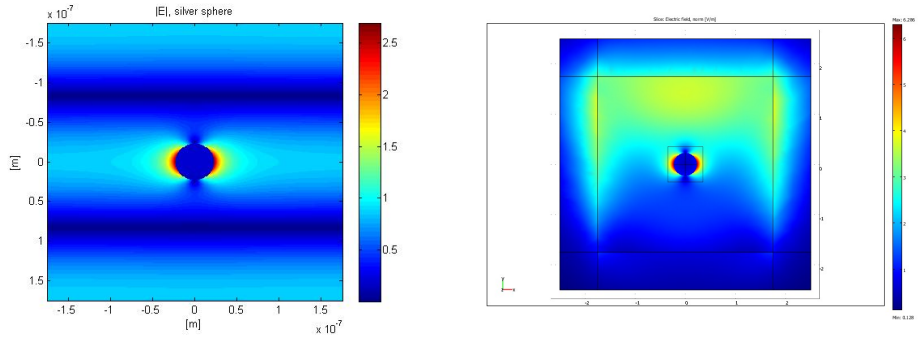

(a) (b)

Figure 9.2: The norm of the electric field calculated using (a) MatLab and (b) Comsol.

The reflections at the edges are even more clear when not including the incident field and only looking at the scattered field in figure 9.3. In the theoretical case scattering will only occur at the sphere. In the simulation there is also a lot of scattering happening at the boundaries.

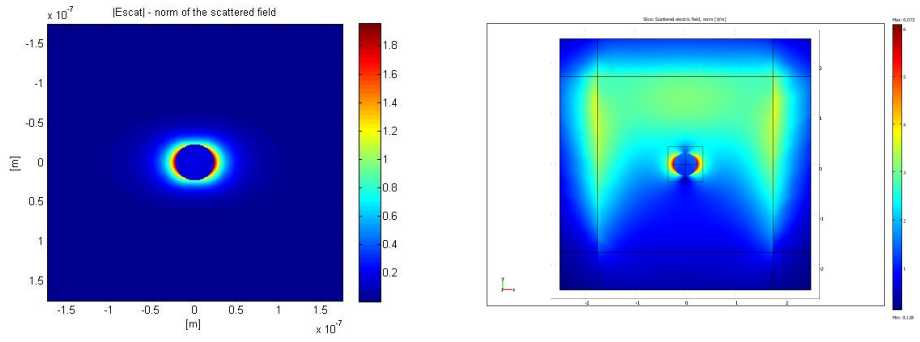

(a) (b)

Figure 9.3: The scattered electric field calculated using (a) MatLab and (b) Comsol.

One way to handle the reflections is to create a reference model without the sphere and only look at the fields relative to this reference. In figure 9.4 the norm of the electric field is plotted along a line cutting the sphere 10 nm from the center. The reference values obtained simply by removing the sphere and re-doing the simulation and the calculation are also shown.

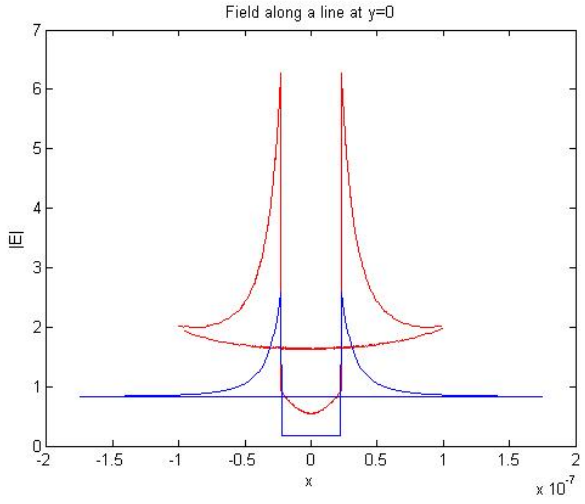

Figure 9.4: Norm of the electric field 20 nm from the center of the sphere along the x-axis, and for a reference model without the sphere. The red line marks simulated data and the blue line theoretically calculated data.

By normalizing the values with respect to the reference model the simulation and the calculation show much more similar results, as is shown in figure 9.5. This is an easy way of removing some of the unwanted effects from the boundaries. The result is better but there is still a discrepancy of about 20 % in the peaks. The enhancement given by the simulations should be interpreted with this in mind.

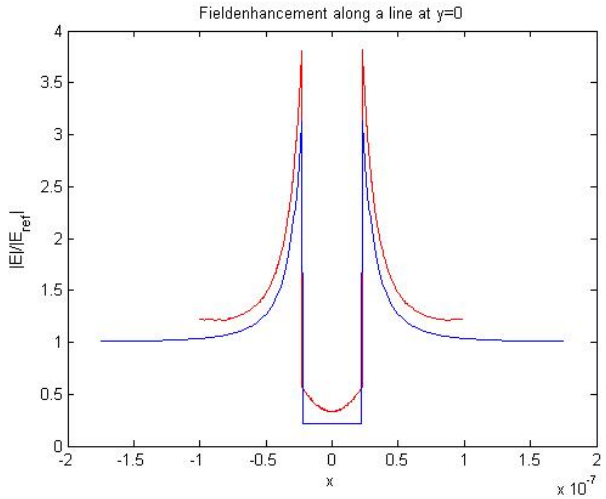

Figure 9.5: Enhancement of the electric field relative to the reference value at x=0. The red line marks simulated data and the blue line theoretically calculated data.

Chapter 10

Design of an optical bowtie antenna

The aim for this thesis is to design an optical antenna for the purpose of entangling remote ions. There are a number of parameters that can be optimized to give the desired properties of the antenna.

The material of the antenna should be chosen to get a low loss. Silver and gold are most widely used for optical antennas since they are easy to manipulate on small scales and have their plasmon resonances within the visible spectrum. Both silver and gold follow the Drude model down to rather short wavelengths. Interband transitions that would increase the absorption drastically does not occur for wavelengths above 650 nm for gold and 400 nm for silver. Silver has the lower absorption and is for that reason chosen as the material for this antenna.

The shape and size of the antenna should be optimized to get a localized surface plasmon resonance for a free space wavelength of 600 nm and as high field strength and large penetration depth as possible. A bowtie antenna has been proven to be a good choice for focusing an electromagnetic field down to a sub wavelength spot. The edges of the bowtie are rounded off to a radius of about 5 nm to eliminate non-local optical response and to give a more realistic shape.

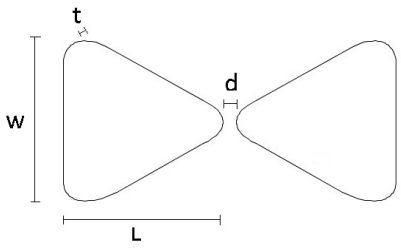

Figure 10.1: The shape and size of the bowtie is determined by it's length (L), width (w), thickness (t) and distance between the antenna elements (d).

The design is done by simulating an antenna for different lengths, widths, thicknesses and gap sizes.

10.1 Length

A bowtie antenna was simulated in Comsol to find the resonant antenna lengths at a free space wavelength of $\lambda_0 = 600$ nm. Other parameters were kept constant:

$w = 20$ nm

$t = 10$ nm

$d = 10$ nm

The result of the simulations is shown in figure 10.2.

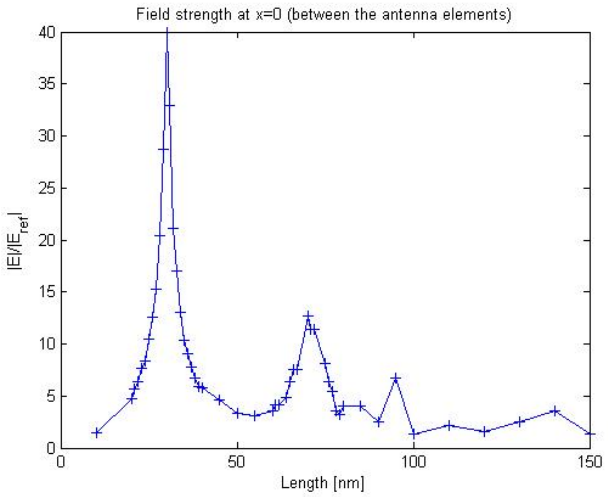

Figure 10.2: Field enhancement at the crystal surface for different lengths of the antenna elements.

There are three resonances showing. The first and largest resonance occurs for a length of 30 nm. This is a good choice for high field enhancement.

10.2 Gap size

Since the RAM memory of the computer limits the mesh size to about 2 nm at the antenna it's not possible to obtain a trustworthy result from simulations for distances smaller than about 4 nm. In figure 10.3 the result is shown for a gap size down to 5 nm. The following constant parameters were used:

$L = 30$ nm

$w = 30$ nm

$t = 10$ nm

By plotting the same data with logarithmic scale on both axis we obtain an approximately linear curve and can confirm that the field enhancement increases exponentially as the gap size decreases. This can be seen in figure 10.4.

By fitting an exponential curve to data it is possible to extrapolate and find the field enhancement for smaller gap sizes. This can be seen in figure 10.5.

Non local optical response is not taken into account in these simulations. When the gap size is very small the electric field will not follow the same pattern as shown above. Electrons will start tunneling over the gap between the antenna elements and destroy the field. At a distance of about 2 nm the effects of non local optical response will be small. I have chosen not to consider distances smaller than 2 nm.

In the following simulations I will use a gap size of 5 nm. When analyzing the antenna in chapter 11 I will estimate the field enhancement for a 2 nm gap size by using an exponential fit in the same way as is done here.

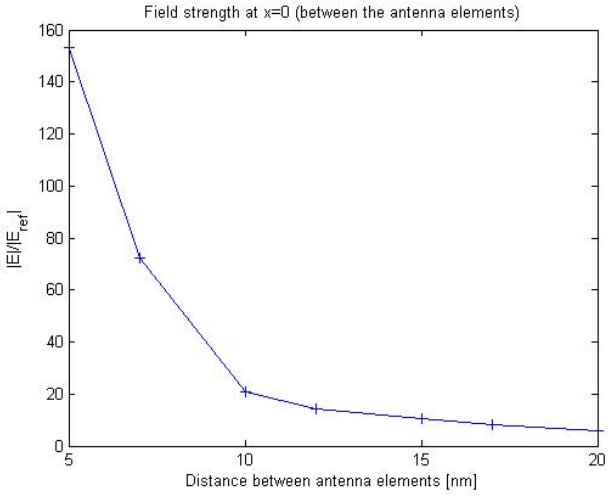

Figure 10.3: Field enhancement at the crystal surface for different gap sizes.

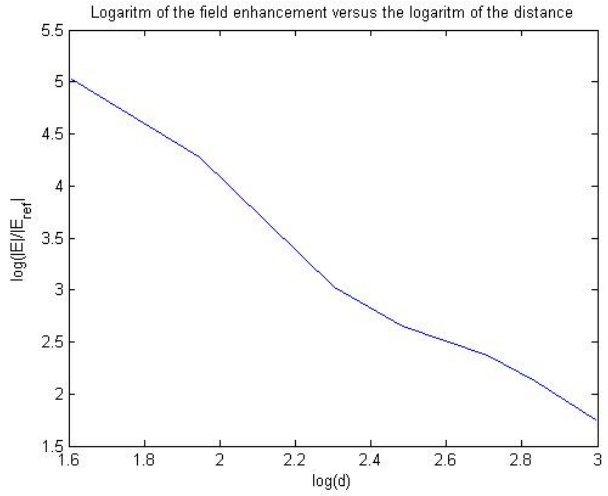

Figure 10.4: Logarithm of the field enhancement versus the logarithm of the gap size.

10.3 Width

Figure 10.6 shows the field enhancement as a function of the width of the antenna. The following constant parameters are used:

$L = 30$ nm

$d = 5$ nm

$t = 10$ nm

Two effects contribute to the field enhancement. First of all a wider antenna will provide more electrons that will oscillate and be squeezed into the sharp edges in the middle. This will give a stronger electric field in the gap. Secondly a wider antenna makes the edge at the gap less sharp which means a lower field enhancement. Instead the outer edges of the antenna will be sharper and give rise to high field strengths.

When changing the width of the antenna the mode structure of the localized surface plasmon will change a lot. In figure 10.7 it can be clearly seen how different shapes of the antenna will give

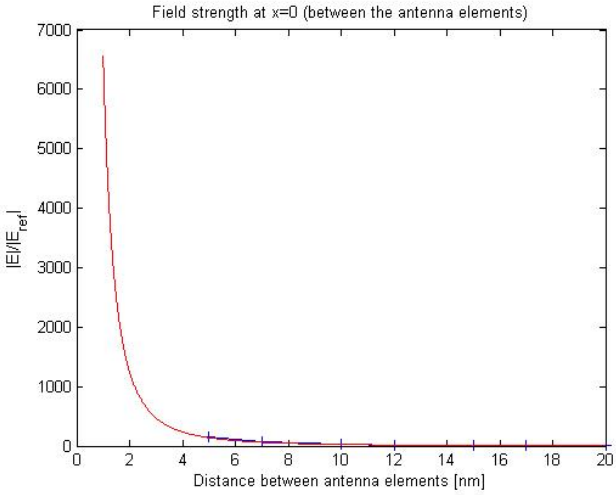

Figure 10.5: Field enhancement as a function of gap size. An exponential curve is fitted to data.

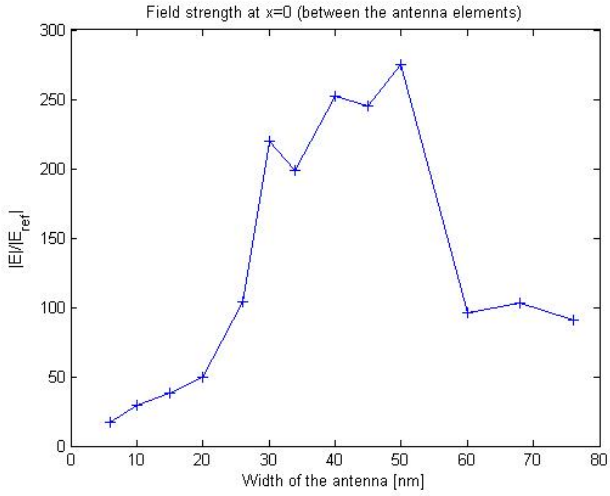

Figure 10.6: Field enhancement at the crystal surface as a function of the width of the antenna.

different field distributions along the antenna. We want a mode structure that gives a high field at the center of the antenna. This will be the case for a width between 30 nm and 55 nm.

I chose to work with a width of 45 nm.

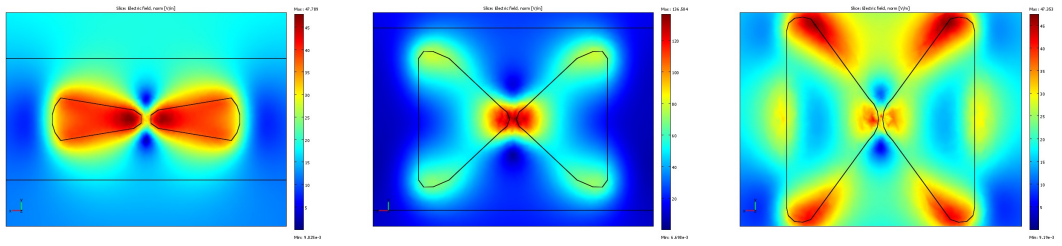

(a) (b) (c)

Figure 10.7: The norm of the electric field 5 nm into the crystal for an antenna width of (a) 15 nm (b) 45 nm and (c) 68 nm.

10.4 Thickness

The thickness of the antenna is varied and the field enhancement is shown in figure 10.8. The constant parameters were set to:

$L = 30$ nm

$d = 5$ nm

$w = 30$ nm

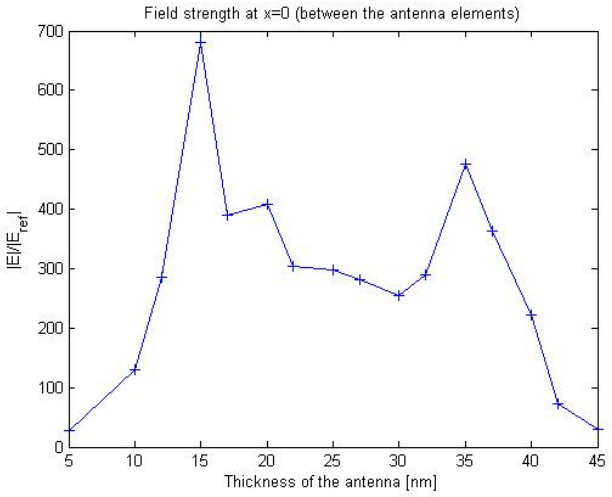

Figure 10.8: Field enhancement at the crystal surface as a function of the thickness of the antenna.

There thickness of the antenna will affect the field enhancement in several different ways. A thicker antenna will change the mode structure of the plasmon wave. As can be seen in figure 10.9, a thicker antenna will give a more focused field.

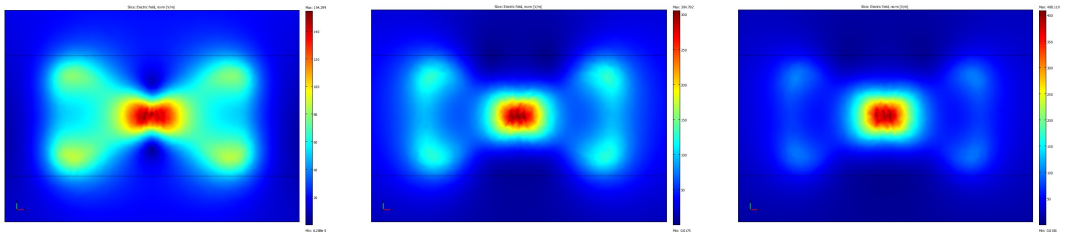

(a) (b) (c)

Figure 10.9: The norm of the electric field 5 nm into the crystal for an antenna thickness of (a) 10 nm (b) 27 nm and (c) 37 nm.

At the same time a thick antenna will shield the crystal surface from the electric field. We want to create a surface plasmon on the interface between the antenna and the crystal, but for a very thick antenna the field will be too low at the crystal surface and there will not be a plasmon resonance. There will then be a larger field enhancement at the top of the antenna, as can be seen in figure 10.10. The contours of the antenna are marked with gray lines and the crystal surface is marked with a red line in the figure.

A thin antenna will focus the field more in the direction perpendicular to the surface of the crystal while the field of a thicker antenna is more spread out along the edges of the antenna.

In figure 10.11 the norm of the electric field is plotted as a function of depth into the crystal for

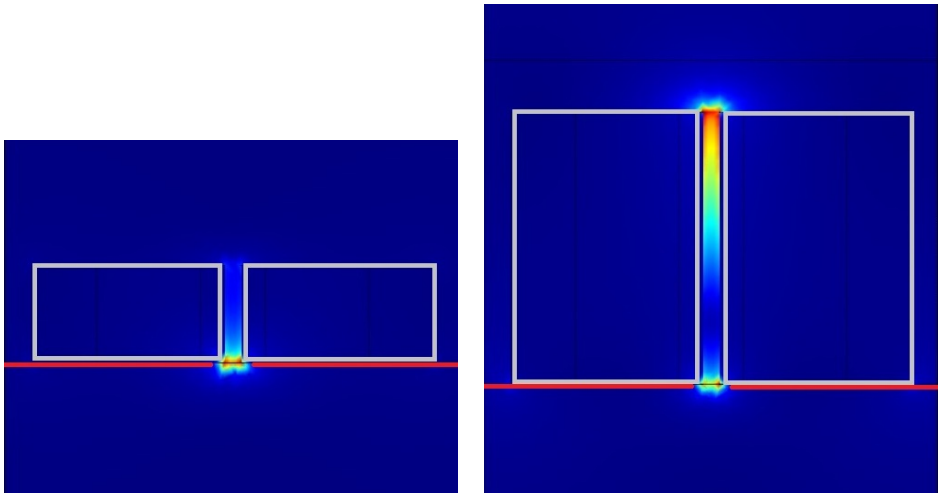

(a) (b)

Figure 10.10: The norm of the electric field along a plane through the center of the antenna perpendicular to the crystal surface for an antenna thickness of (a) 15 nm and (b) 42 nm. The crystal surface is marked with a red line and the antenna with gray lines.

different thicknesses of the antenna. The optimal thickness depends on where in the crystal the entangler ion is sitting. For example at a depth of 15 nm into the crystal a thickness of 30 nm is better than a thickness of 15 nm. The field is however very weak this far into the crystal, probably too weak to work with. For that reason I have chosen the parameters that give the highest field enhancement at the surface of the crystal.

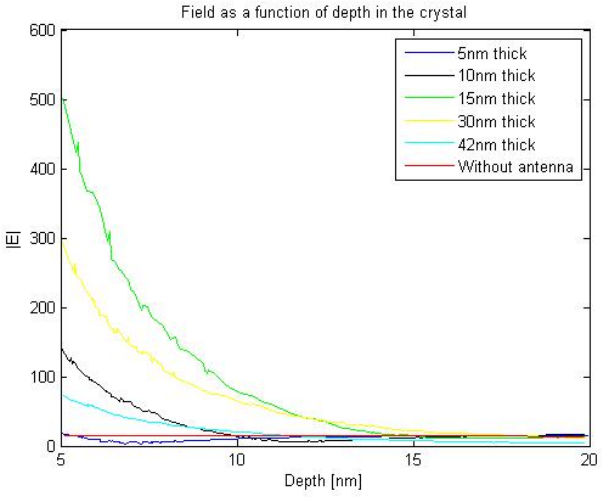

Figure 10.11: Field strength as a function of depth in the crystal.

From simulations it seems like the optimal thickness is somewhere between 15 nm and 35 nm. I have chosen to work with a 15 nm thick antenna.

10.5 Summary

The chosen design is based on a high field enhancement. The penetration depth can also vary with the size and shape of the antenna but in general a higher field at the surface of the crystal will

also imply a higher field inside the crystal. When this is not the case the field is too weak to be useful anyway.

The chosen design parameters are as follows.

Material:	Silver
Length:	30 nm
Gap size:	2 nm
Width:	45 nm
Thickness:	15 nm

Chapter 11

Performance

I this chapter the result of my design will be evaluated. The field distribution in a plane along the crystal surface as well as perpendicular to the crystal surface can be seen in figure 11.1.

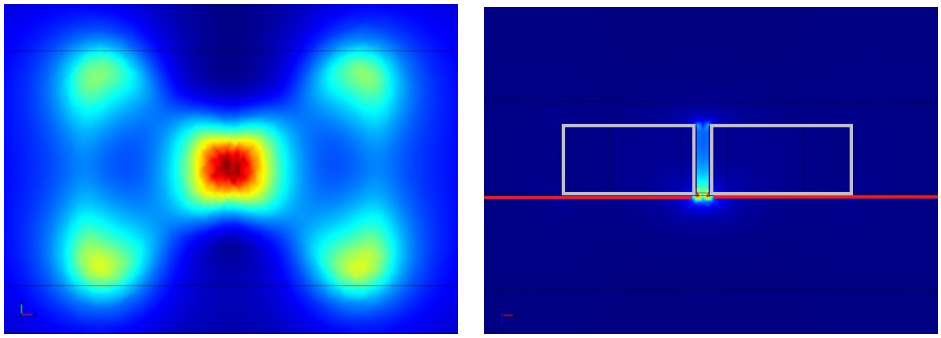

(a) (b)

Figure 11.1: The norm of the electric field 5 nm below the crystal surface (a) and along the normal to the surface (b).

All field enhancements shown in the plots below are relative to a reference field simulated with the same model but without the antenna.

11.1 Field enhancement

The field enhancement along the length of the antenna at the crystal surface is shown in figure 11.2. This result was obtained by using a gap size of 2 nm and a mesh size of 2 nm. Such a coarse mesh can not resolve the gap properly. For that reason the same antenna was simulated for a gap size of 5, 6, 10 and 14 nm. An exponential curve was fitted to data and extrapolated to a gap size of 2 nm. This is shown in figure 11.3. The simulated result for a 2 nm gap with a 2 nm mesh is shown as a black cross just above the marker.

This fitting is very sensitive to errors in the simulations. A small error in one of the simulated values will grow in the extrapolated curve and become a big error for small gap sizes. Despite this, the simulated value for a 2 nm gap matches surprisingly well to the extrapolated curve.

The field enhancement at the crystal surface in the center of the antenna elements is:

$$\frac{|E|}{|E_{ref}|} \approx 1100$$

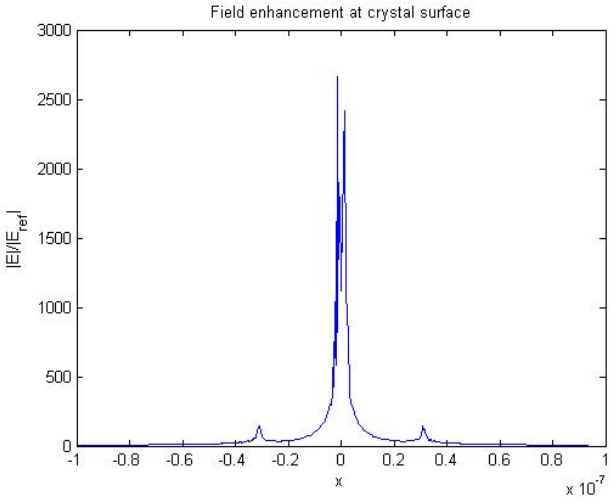

Figure 11.2: Field enhancement along the length of the antenna (the x-axis) at the crystal surface.

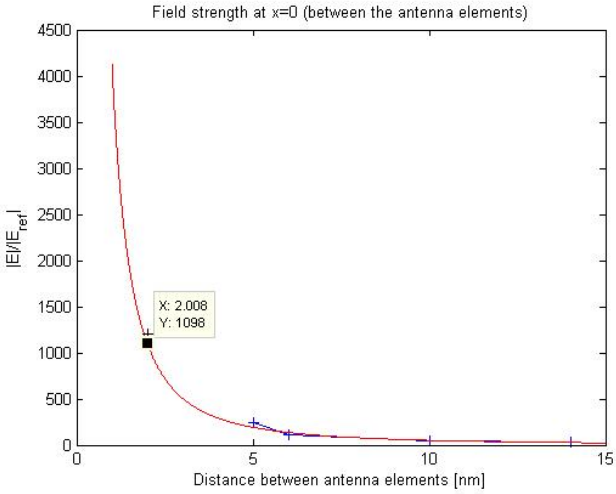

Figure 11.3: Field enhancement as a function of distance between the antenna elements.

According to figure 11.2 the field is larger just below the sharp tips of the antenna. At these spots the field enhancement can be as large as 2700 times the reference field.

11.2 Penetration depth

The field will decay very rapidly inside the crystal, as can be seen in figure 11.4. To achieve an enhancement of 1000 times we can only reach about 1 nm into the crystal. For a field enhancement of 100 times we could reach ions sitting 5 nm into the crystal and if 10 times enhancement is enough we can operate about 14 nm into the crystal.

11.3 Linewidth and lifetime

By modeling the antenna using a Drude model and varying the wavelength of the incident light the linewidth of the resonance peak can be determined. The result is shown in figure 11.5.

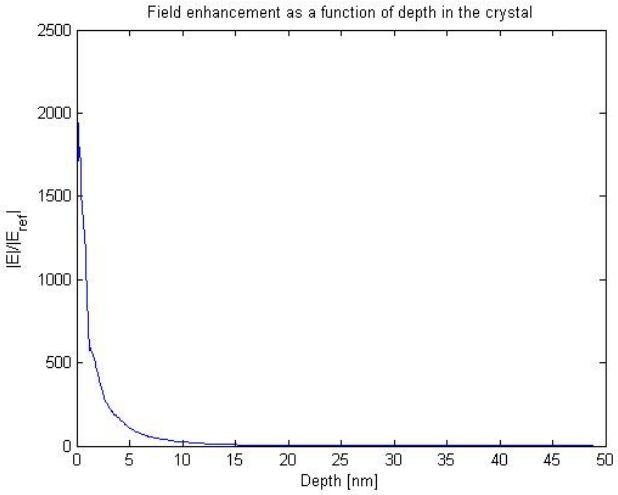

(a)

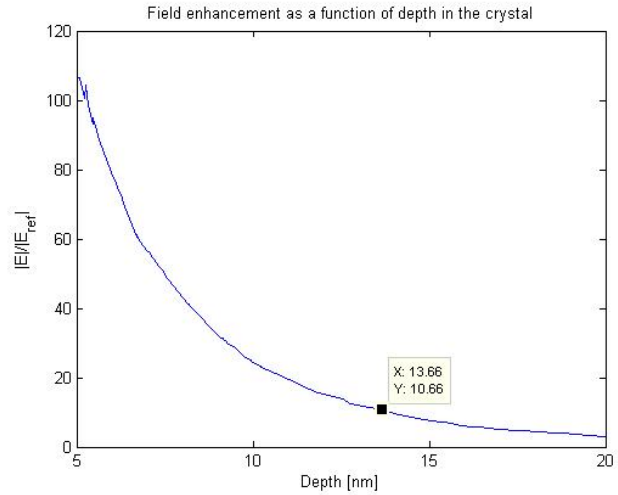

(b)

Figure 11.4: The norm of the electric field as a function of depth into the crystal. Figure (b) is a version of figure (a) zoomed in at the interesting region.

The FWHM is about 40 nm in wavelength and about 35 THz in frequency. Assuming a Lorentzian line shape this gives a lifetime of the antenna:

$$\tau = \frac{1}{\pi \Delta \nu} \approx 9.1\text{fs}$$

11.4 Polarization dependence

We want the antenna to be sensitive to the polarization of the incoming light. The antenna was simulated for the opposite polarization compared to the optimal case presented above, with the electric field along the thickness of the antenna in the z-direction (TM-polarized). The resulting field enhancement at the surface of the crystal is shown in figure 11.6.

The maximum field enhancement is less than 7 times the reference field. This is a lot less than for TE-polarized light.

With a field enhancement this small it is very unlikely that an ion will absorb the incoming photon.

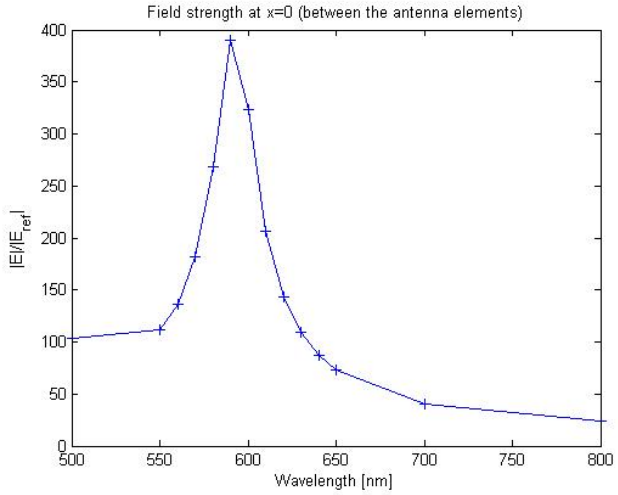

Figure 11.5: Field enhancement as a function of wavelength.

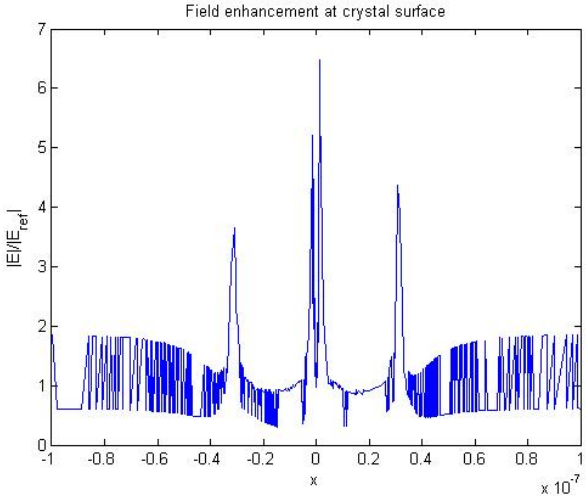

Figure 11.6: Field enhancement at the crystal surface along the length of the antenna for TM-polarized light.

There is still a risk that the photon will be absorbed in the metal of the antenna and that we will not be able to detect it. Since the antenna is not resonant for this polarization the absorption and scattering probability will be lower than for the TE-polarized case. Again it is very hard to say how big the absorption probability will be, since it depends on the coupling between the microresonator and the antenna.

11.5 Error sources

The model used for simulations is not perfect. The boundaries of the geometry cause reflections that will interfere with the incoming field and the field scattered by the antenna. The situation can be improved by using a reference model without the antenna and relating all results to this reference. There is still some uncertainty in the values given and they should be viewed as an indication of what we can achieve using an optical antenna rather than the absolute truth.

The mesh is critical for resolving small details in the model. I have used a mesh about half the size

of the smallest details in my model. A finer mesh is desirable to obtain correct values. Considering simulations made for different sizes of the mesh compared to other sources of error I don't think the size of the mesh is the limiting factor in this case. The location of the nodes can also influence the solution, especially for a rather coarse mesh. If the point of interest is close to a nodal point the error will be smaller than if we are far away from a nodal point. In this case we are often interested in the field in the center of the antenna gap. With only two mesh elements to resolve the gap the placement of the nodal point might be critical.

Very sharp edges can cause singularities and unrealistic high fields in a simulation. I have tried to avoid sharp edges by rounding off the corners of the antenna. Since the antenna is flat there are still sharp edges around the upper and lower surfaces of the antenna. From the look of the result this doesn't seem to be a problem, but it's difficult to know exactly what the effect is.

Chapter 12

Discussion and further considerations

Some of the results given in the previous section will be discussed in this chapter.

There are plenty of questions not answered within the scope of this project. There are also a few problems with this approach to scalability of a rare-earth quantum computer that are not solved yet. I will briefly discuss some of the problems and questions not investigated in detail within this thesis.

12.1 Importance of design parameters

The length of the antenna is critical to obtain a localized plasmon polariton resonance. The length of the antenna elements must be determined with an accuracy of at least 10 nm.

The size of the gap between the antenna elements is also critical to obtain a high field strength. This is probably the most important parameter. The field strength increases exponentially with a smaller gap size, until the gap size is so small that we have to take non local optical response into account.

The thickness and width of the antenna are not so critical. This is illustrated by the fact that the field enhancement using a width of 30 nm and a thickness of 10 nm in figure 10.5 is practically the same as the field enhancement for the optimized antenna in figure 11.3. The thickness and width will affect the mode structure of the antenna and this can also have an effect on the penetration depth.

12.2 Effect on the lifetime of the ions

The presence of a metal structure close to the ions will not only enhance the absorption but also the emission of the ions. An increased emission implies a shorter lifetime.

By using an entangler ion with a resonance frequency different from the resonance frequency of the qubit ions we could design an antenna that is only resonant for the entangler ion frequency but not for the qubits. In that way we could limit the influence of the antenna on the qubits. The resonance wavelength of the entangler ion would have to be separated from the qubit wavelength by more than 50 nm to keep the qubit ions outside the resonance peak. The antenna has more than one resonance peak and would need to be designed such that the qubits are unaffected by all peaks.

The antenna will increase the emission of the entangler ion and decrease it's lifetime. This is a problem that is very difficult to get around. This effect would have to be investigated in more

detail.

12.3 Penetration depth

The penetration depth for the field into the crystal is very small. This is a problem if we want to place an entangler ion inside the crystal, where it is shielded from the environment. Depending on how big field enhancement we need we can operate from the surface of the crystal and down to a maximum depth of about 14 nm. This is probably not enough.

The coherence properties of ions close to the surface of the crystal would need to be investigated to see how far into the crystal we need to operate.

12.4 Losses

The antenna has an estimated lifetime of 9.1 fs based on the simulated linewidth. This is a very short lifetime compared to the interaction time.

It is difficult to say how the short lifetime of the antenna will affect the system as a whole. At each time the incoming photon will be in a superposition between a photon in the cavity, a plasmon in the antenna and absorbed by the ion. How much losses the antenna will introduce in the system depends on how big part of the photon that is in the antenna at each time, or equivalently how much time the photon spends in the antenna during the process. My guess is that the losses will be rather big. This will also need to be investigated further.

12.5 Polarization dependence

We want the antenna to be very sensitive to polarization so that a TE-polarized photon will be absorbed by an ion with a high probability and a TM-polarized photon will pass by unaffected and be detected after passing a beam splitter. Simulations indicate that the antenna is indeed very polarization sensitive and will not give a high field enhancement for TM-polarized light.

One of the things that need to be investigated further is how a toroidal microresonator will affect the polarization state of a photon. We need the polarization to be preserved through the whole setup.

There are other difficulties arising if we want to detect the remaining photon after the beam splitter of the setup. Even if the field enhancement is not very big there might still be a risk that the photon will be absorbed by the antenna. At this stage it is difficult to say how big the absorption probability is.

12.6 Refractive index mismatch

To achieve a strong field in the crystal we need to put it as close to the surface of the microresonator as possible. There is one problem arising because of the high refractive index of the crystal. The index of refraction is higher in the crystal than in a common silica microresonator, and this can cause a leakage of the field from the resonator into the crystal. This can reduce the lifetime of the resonator significantly. The problem could be solved by making the toroidal microresonator from a higher index material ($n>1.8$).

12.7 Making a plasmonic antenna

Electron beam lithography is a powerful and versatile way to create small metal structures. It was developed to manufacture integrated circuits but has proven to be very useful also within nano technology. A surface is first covered by a so called resist. An electron beam is swept over the parts of the surface where the metal should be placed. The resist is removed in this part in a development process. A thin metal layer can then be evaporated onto the surface. After the rest of the resist is removed only the metal in the parts swept by the electron beam remains, [43].

With electron beam lithography it seems possible to make an optical antenna on a crystal surface. The metal need to be made as thin as 15 nm. The smallest details and sharpest edges possible have in this thesis been assumed to be 5 nm. This is probably on the limit for what is possible using electron beam lithography.

The biggest challenge when manufacturing the antenna designed in this work would probably be the small gap between the antenna elements. When the resist is removed after evaporation there is a risk that some metal will still remain in the gap between the antenna elements.

The gap size has a big influence on the field enhancement and metal in the gap will cause a short circuit and destroy the field. Different ways of removing the metal in a very thin gap between the antenna elements could be investigated.

Chapter 13

Conclusion and outlook

With an optical antenna it is possible to focus light down to sub-wavelength spots and the field enhancement can be very large. The most critical design parameters are the length and gap size of the antenna. With the design given in this thesis simulations gave a field enhancement of 1100 times in the center of the antenna at the surface of the crystal. The maximum field enhancement at the surface of the crystal occurred just below the sharp tips of the antenna and was about 2700 times the reference.

The field enhancement is enough to create a single photon pi-pulse from the evanescent field of a microresonator for an ion at the surface of a crystal. Depending on the microresonator it might be possible to create a pi-pulse up to a depth of 14 nm into the crystal.

The plasmonic antenna designed in this thesis is only resonant for a TE-polarized field. A photon of the opposite polarization will have a much higher probability to pass by unaffected. This is very promising for the proposed idea to entangle remote ions by using entangled photon pairs.

There are several difficulties with using a plasmonic antenna to entangle ions in two different crystals. We can not enhance the field very far into the crystal and hence not use ions very far into the crystal structure.

In a quantum computer good quantum control and coherence are very important features. The presence of an antenna will disturb the system and make it hard to keep the coherence and control.

There are however several open questions remaining. If it would be possible to use ions sitting very close to the surface of a crystal using a plasmonic antenna might still be a way to entangle remote ions.

With an increasing ability to fabricate high-Q microresonators as well as nano-structures tailored to manipulate light in different ways it is in my opinion very probable that we in the future will be able to entangle remote ions. This would be a big step towards a working rare-earth-ion quantum computer.

Acknowledgments

Many thanks to my supervisor Stefan Kröll for much help, feedback and encouragement during the year and also for bringing me into an exciting field of physics and a great group of colleagues. I would also like to thank the rest of the Quantum Information Group for plenty of inspiring conversations and lunches.

This project would not have been possible without the support of Daniel Sjöberg at Electrical and Information Technology, who helped me with modeling and understanding electromagnetic fields and plasmonics. Many thanks for discussions, quick help by email and for leading me through the Comsol Multiphysics jungle.

I am very grateful to all people at the division of Atomic Physics for providing an inspiring and social environment. Working hard is a lot easier with a good cup of coffee and a bunch of nice people around.

Bibliography

[1] P.W. Shor, *Polynomial-time algorithms for prime factorization and discrete logarithms on a quantum computer*, Siam J. Comput. **26**, 1484-1509 (1997)

[2] B. Qi, L. Qian, H-K. Lo, *A brief introduction of quantum cryptography for engineers*, arXiv:1002.1237 [quant-ph], (2010)

[3] D. P. DiVincenzo, *The Physical Implementation of Quantum Computation*, arXiv:quant-ph/0002077v3, (2000)

[4] I. L. Chuang,L. M. K. Vandersypen, X. Zhou, D. W. Leung, S. Lloyd, *Experimental realization of a quantum algorithm*, Nature, **393**, 143-146, (1998)

[5] J. A. Jones,M. Mosca, R. H. Hansen, *Implementation of a quantum search algorithm on a quantum computer*, Nature, **393**, 344-346, (1998)

[6] S. Guide et al. *Implementation of the Deutsch-Jozsa algorithm on an ion-trap quantum computer*, Nature, **421**, 48-50, (2003)

[7] K-A. Brickman et al. *Implementation of Grover's quantum search algorithm in a scalable system*, Phys. Rev. A, **72**, 050306(R), (2005)

[8] P. G. Kwiat, J. R. Mitchell, P. D. D. Schwindt, A. G. White, *Grover's search algorithm: an optical approach*, J. Mod. Opt. **47**, 257-266, (2000)

[9] L.M.K. Vandersypen, M. Steffen, G. Breyta, C.S. Yannoni, M.H. Sherwood, I. Chuang, *Experimental realization of Shor's quantum factoring algorithm using nuclear magnetic resonance*, Nature, **414**, 883-887, (2001)

[10] B. P. Lanyon, T. J. Weinhold, N. K. Langford, M. Barbieri, D. F. V. James, A. Gilchrist, A. G. White, *Experimental demonstration of Shor's algorithm with quantum entanglement*, Phys. Rev. Lett., **99**, 250505, (2007)

[11] L. DiCarlo, J. M. Chow, J. M. Gambetta, L. S. Bishop, B. R. Johnson, D. I. Schuster, J. Majer, A. Blais, L. Frunzio, S. M. Girvin, R. J. Schoelkopf, *Demonstration of two-qubit algorithms with a superconducting quantum processor*, Nature, **460**, 240-244, (2009)

[12] N. Ohlsson, R. K. Mohan, S. Kröll, *Quantum computer hardware based on rare-earth-ion-doped inorganic crystals*, Opt. Comm.,**201**, 71-77, (2002)

[13] A. Walther, B. Julsgaard, L. Rippe, Y. Ying, S. Kröll, *Extracting high fidelity quantum computer hardware from random systems*, arXiv:1001.1664v1 [quant-ph], (2010)

[14] M. Nilsson, *Coherent Interactions in rare-Earth-Ion-doped Crystals for Applications in Quantum Information Science*, PhD thesis, Division of Atomic Physics, LTH, (2004)

[15] M. Nilsson, L. Rippe, S. Kröll, *Hole-burning techniques for isolation and study of individual hyperfine transitions in inhomogeneously broadened solids demonstrated in* $Pr^{3+}:Y_2SiO_5$, Phys. Rev. B, **70**, 214116, (2004)

[16] I. Roos, K. Mølmer, *Quantum computing with an inhomogeneously broadened ensemble of ions: Suppression of errors from detuning variations by specially adapted pulses and coherent population trapping*, Phys. Rev. A, **69**, 022321, (2004)

[17] L. Rippe, M. Nilsson, S. Kröll, R. Klieber, D. Suter, *Experimental demonstration of efficient and selective population transfer and qubit distillation in a rare-earth-metal-ion-doped crystal*, Phys. Rev. A, **71**, 062328, (2005)

[18] J.H. Wesenberg, K. Mölmer, L. Rippe, S. Kröll, *Scalable designs for quantum computing with rare-earth-ion-doped crystals*, Phys. Rev. A, **75**, 012304, (2007)

[19] J. J. Longdell, M. J. Sellars, *Experimental demonstration of quantum-state tomography and qubit-qubit interactions for rare-earth-metal-ion-based solid-state qubits*, Phys. Rev. A, **69**, 032307, (2004)

[20] L. Rippe, B. Julsgaard, A: walther, Y. Ying, S. Kröll, *Experimental quantum state tomography of a solid state qubit*, Phys. Rev. A, **77**, 022307, (2008)

[21] L. Jiang, J. M. Taylor, A. S. Sorensen, M. D. Lukin, *Distributed quantum computation based on small quantum registers*, Phys. Rev. A, **76**, 062323, (2007)

[22] C.J. Foot, *Atomic Physics*, Oxford University Press, (2004)

[23] S. M. Spillane, T. J. Kippenberg, O. J. Painter, K. J. Vahala, *Ideality in a Fiber-Taper-Coupled Microresonator System for Application to Cavity Quantum Electrodynamics*, Phys. Rev. Let., **91**, 043902, (2003)

[24] S.M. Spillane, T.J. Kippenberg, K.J. Vahala, K.W. Goh, E. Wilcut, H.J. Kimble, *Ultrahigh-Q toroidal microresonators for cavity quantum electrodynamics*, Phys. Rev. A, **71**, 013817, (2005)

[25] T. Aoki, B. Dayan, E. Wilcut, W.P. Bowen, A.S. Parkins, T.J. Kippenberg, K.J. Vahala, H.J. Kimble, *Observation of strong coupling between one atom and a monolithic microresonator*, Nature, **443**, 671, (2006)

[26] D. A. Steck, *Cesium D Line Data*, http://steck.us/alkalidata/cesiumnumbers.1.6.pdf, (1998)

[27] S. Maier, *Plasmonics: Fundamentals and Applications*, Springer, Berlin, (2007)

[28] E.J. Heilweil, R. M. Hochstrasser, *Nonlinear spectroscopy and picosecond transient grating study of colloidal gold*, J. Chem. Phys., **82**, 4762, (1985)

[29] M. Scandurra, *Quantum vacuum pressure on a conducting slab*, arXiv:hep-th/0307150v1, (2003)

[30] S. J. Orfanidis, *Electromagnetic waves and antennas*, www.ece.rutgers.edu/ orfanidi/ewa, (1996)

[31] P. Drude, *Zur Elektronentheorie der Metalle*, Ann. Phys. **1**, 566, (1900)

[32] G. Kristensson, *Elektromagnetisk vågutbredning*, Studentlitteratur, (1999)

[33] J.D. Jackson, *Classical Electrodynamics*, 3rd ed, John Wiley and Sons, New York, (1999)

[34] C. Sönnichsen, T. Franzl, T. Wilk, G. von Plessen, J. Feldmann, O. Wilson, P. Mulvaney, *Drastic reduction of plasmon damping in gold nanorods*, Phys. Rev. Lett., **88**, 077402, (2002)

[35] 1.M. Svedendahl, S. Chen, A. Dmitriev, M. Käll, *Refractometric Sensing Using Propagating versus Localized Surface Plasmons: A Direct Comparison*, Nano Lett., **9**, 4428-4433, (2009)

[36] J. Li, D. Fattal, Z. Li, *Plasmonic optical antennas on dielectric gratings with high field enhancement for surface enhanced Raman Spectroscopy*, Appl. Phys. Lett., **94**, 263114, (2009)

[37] R. D. grober, R. J. Schoelkopf, D. E. Prober, *Optical antenna: Towards a unity efficiency near-field probe*, Appl. Phys. Lett., **70**, 1354, (1997)

[38] A. Sundaramurthy, K. B. Crozier, G. S. Kino, D. P. Fromm, P. J. Schuck, W. E. Moerner, *Field enhancement and gap-dependent resonance in a system of two opposing tip-to-tip Au nanotriangles*, Phys. Rev. B, **72**, 165409, (2005)

[39] H. Guo, T. P. Meyrath, T. Zentgraf, N. Liu, L. Fu, H. Schweizer, H. Giessen, *Optical resonances of bowtie slot antennas and their geometry and material dependence*, Opt. Exp., **16**, 7756, (2008)

[40] K. Cho, *Optical response of nanostructures, Microscopic non-local theory*, Springer-Verlag, Berlin Heidelberg, (2003)

[41] Y. C. Sun, *Rare Earth Materials in Optical Storage and Data Processing Applications, Chapter 7: Rare Earth Materials in Optical Storage and Data Processing Applications*, Springer-Verlag, Berlin Heidelberg, (2005)

[42] N. Ottosen, H. Petersson, *Introduction to the Finite Element Method*, Prentice Hall Europe, London, (1992)

[43] E. Lorek, *Electron Beam Lithography and Evaporation on Ultra-thin Silicon Nitride Membranes - Target Manufacturing for Digital Holography*, Lund Reports On Atomic Physics LRAP-416, (2010)

Appendix A

Conditions for propagating SPP's confined to a metal surface

I want to investigate if a surface wave can propagate along a metal-dielectric interface. I will follow [27] rather closely. The investigation will make use of Maxwells equations:

$$\nabla \cdot \mathbf{D} = \rho_{ext} \tag{A.1}$$

$$\nabla \cdot \mathbf{B} = 0 \tag{A.2}$$

$$\nabla \times \mathbf{E} = -\frac{\partial \mathbf{D}}{\partial t} \tag{A.3}$$

$$\nabla \times \mathbf{H} = \mathbf{J}_{ext} + \frac{\partial \mathbf{D}}{\partial t} \tag{A.4}$$

We choose to place the interface between a metal layer and an insulator at z=0 in a cartesian coordinate system, and assume that the wave is propagating in the x-direction. We also assume that the fields are constant in the y-direction to get an easier 2-dimensional problem.

$$\mathbf{E}(t, \mathbf{r}) = \mathbf{E}(t, z)e^{ik_x x}$$

where $\mathbf{E}(t, z) = \mathbf{E}(z)e^{-i\omega t}$. By assuming a similair form of the magnetic field and putting this into Maxwell's equations A.3, A.4, we get the following system of equations [27]:

$$\left(\frac{\partial E_z}{\partial y} - \frac{\partial E_y}{\partial z}, \frac{\partial E_x}{\partial z} - \frac{\partial E_z}{\partial x}, \frac{\partial E_y}{\partial x} - \frac{\partial E_x}{\partial y}\right) = \left(-\frac{\partial E_y}{\partial z}, \frac{\partial E_x}{\partial z} - ik_x E_z, ik_x E_y\right) = i\omega\mu_0 \left(H_x, H_y, H_z\right) \tag{A.5}$$

$$\left(\frac{\partial H_z}{\partial y} - \frac{\partial H_y}{\partial z}, \frac{\partial H_x}{\partial z} - \frac{\partial H_z}{\partial x}, \frac{\partial H_y}{\partial x} - \frac{\partial H_x}{\partial y}\right) = \left(-\frac{\partial H_y}{\partial z}, \frac{\partial H_x}{\partial z} - ik_x H_z, ik_x H_y\right) = -i\omega\epsilon_0\varepsilon \left(E_x, E_y, E_z\right) \tag{A.6}$$

There are two types of solutions to the system of equations above. The first case is a TM-polarized wave ($H_z = 0$) with the magnetic field along the interface and the second case is a TE-polarized wave ($E_z = 0$) with the electric field along the interface .

For the TE-case we get by using A.5 and $H_y = 0$:

$$H_x = i\frac{1}{\omega\mu_0}\frac{\partial E_y}{\partial z}$$

$$H_z = \frac{k_x}{\omega\mu_0}E_y$$

Combining this with A.6 and using $k_0 = \frac{\omega}{c_0} = \omega\sqrt{\epsilon_0\mu_0}$:

$$\frac{\partial^2 E_y}{\partial z^2} + (\varepsilon k_0^2 - k_x^2)E_y = 0$$

$$E_x = E_z = 0$$

Defining $k_z^2 = \varepsilon k_0^2 - k_x^2$ (the z-component of the wavevector in each material), we get for $z < 0$:

$$E_y = A_1 e^{-ik_{z1}z}$$

$$H_x = \frac{k_{z1}}{\omega\mu_0} A_1 e^{-ik_{z1}z}$$

$$H_z = \frac{k_x}{\omega\mu_0} A_1 e^{-ik_{z1}z}$$

Similarly for $z > 0$:

$$E_y = A_2 e^{ik_{z2}z}$$

$$H_x = -\frac{k_{z2}}{\omega\mu_0} A_2 e^{ik_{z2}z}$$

$$H_z = \frac{k_x}{\omega\mu_0} A_2 e^{ik_{z2}z}$$

Boundary conditions require that E_y and H_x are continuous across the boundary.

$$A_1 = A_2$$

$$k_{z1} = -k_{z2}$$

If the wave decays exponetially on one side of the surface, $z < 0$ say, $\mathrm{Im}k_{z1} < 0$. Then $\mathrm{Im}k_{z2} > 0$ and the wave is not confined to the surface for $z > 0$. Thus, a TE-polarized surface wave is not possible!

For the TM-case, with $E_y = 0$:

$$E_x = -i\frac{1}{\omega\epsilon_0\varepsilon}\frac{\partial H_y}{\partial z}$$

$$E_z = -\frac{k_x}{\omega\epsilon_0\varepsilon} H_y$$

$$\frac{\partial^2 H_y}{\partial z^2} + (\varepsilon k_0^2 - k_x^2)H_y = 0$$

$$H_x = H_z = 0$$

The solution for $z < 0$ is:

$$H_y = B_1 e^{-ik_{z1}z}$$

$$E_x = -\frac{k_{z1}}{\omega\epsilon_0\varepsilon_1} B_1 e^{-ik_{z1}z}$$

$$H_z = -\frac{k_x}{\omega\epsilon_0\varepsilon} B_1 e^{-ik_{z1}z}$$

And for $z > 0$:

$$H_y = B_2 e^{ik_{z2}z}$$

$$E_x = \frac{k_{z2}}{\omega\epsilon_0\varepsilon_2} B_2 e^{ik_{z2}z}$$

$$H_z = -\frac{k_x}{\omega\epsilon_0\varepsilon} B_2 e^{ik_{z2}z}$$

Boundary conditions require that H_y and εE_x are continuous across the boundary.

$$B_1 = B_2$$

$$\frac{k_{z1}}{\varepsilon_1} = -\frac{k_{z2}}{\varepsilon_2}$$

Dividing this expression into a real and an imaginary part we get:

$$\frac{\mathrm{Re}(k_{z1})\mathrm{Re}(\varepsilon_1) + \mathrm{Im}(k_{z1})\mathrm{Im}(\varepsilon_1)}{|\varepsilon_1|^2} = -\frac{\mathrm{Re}(k_{z2})\mathrm{Re}(\varepsilon_2) + \mathrm{Im}(k_{z2})\mathrm{Im}(\varepsilon_2)}{|\varepsilon_2|^2}$$

$$\frac{\mathrm{Im}(k_{z1})\mathrm{Re}(\varepsilon_1) - \mathrm{Re}(k_{z1})\mathrm{Im}(\varepsilon_1)}{|\varepsilon_1|^2} = -\frac{\mathrm{Im}(k_{z2})\mathrm{Re}(\varepsilon_2) + \mathrm{Re}(k_{z2})\mathrm{Im}(\varepsilon_2)}{|\varepsilon_2|^2}$$

Assuming that $\mathrm{Im}(\varepsilon) << \mathrm{Re}(\varepsilon)$ for both materials and demanding that $\mathrm{Im}k_{z1} < 0$ and $\mathrm{Im}k_{z2} < 0$ for a confined mode we see that $\mathrm{Re}(\varepsilon_1)$ and $\mathrm{Re}(\varepsilon_2)$ must have different signs.

If for example $\varepsilon_1 > 0$ and $\varepsilon_2 < 0$ the interface between the two materials can support a propagating surface plasmon polariton with a certain wavevector $k_x = k_{x1} = k_{x2}$.